O. Gil-Castell, N. Mascia, C. Primaz, F. Vásquez-Garay, M.G. Baschetti, A. Ribes-Greus. Brewer's spent grains as biofuels in combustion-based energy recovery processes: Evaluation of thermo-oxidative decomposition. Fuel, 2022; 312(122955)

Conductive polycaprolactone/gelatin/polyaniline nanofibres as functional scaffolds for cardiac tissue regeneration

O. Gil-Castell[1], I. Ontoria-Oviedo[2], J.D. Badia[3], E. Amaro-Prellezo[2], P. Sepúlveda[2], A. Ribes-Greus[1,*]

DOI: https://doi.org/10.1016/j.reactfunctpolym.2021.105064

Please, cite it as: O. Gil-Castell, I. Ontoria-Oviedo, J.D. Badia, E. Amaro-Prellezo, P. Sepúlveda, A. Ribes-Greus. Conductive polycaprolactone/gelatin/polyaniline nanofibres as functional scaffolds for cardiac tissue regeneration: Reactive and Functional Polymers, 2022; 105064

1. Instituto de Tecnología de Materiales (ITM), Universitat Politècnica de València (UPV), Camino de Vera S/n, 46022, Valencia, Spain.
2. Unidad de Regeneración y Trasplante Cardíaco, Instituto de Investigación Sanitaria La Fe, Av. Fernando Abril Martorell Torre A, 46026, Valencia, Spain
3. Departament d'Enginyeria Química, Escola Tècnica Superior d'Enginyeria, Universitat de València, Av. de la Universitat, s/n, 46100 Burjassot, Spain

*Corresponding author: aribes@ter.upv.es

O. Gil-Castell, N. Mascia, C. Primaz, F. Vásquez-Garay, M.G. Baschetti, A. Ribes-Greus. Brewer's spent grains as biofuels in combustion-based energy recovery processes: Evaluation of thermo-oxidative decomposition. Fuel, 2022; 312(122955)

Conductive polycaprolactone/gelatin/polyaniline nanofibres as functional scaffolds for cardiac tissue regeneration

O. Gil-Castell[1], I. Ontoria-Oviedo[2], J. D. Badia[3], E. Amaro-Prellezo[2], P. Sepúlveda[2], A. Ribes-Greus[1,*]

[1]Instituto de Tecnología de Materiales (ITM). Universitat Politècnica de València. Camino de Vera s/n, 46022 Valencia, Spain

[2]Unidad de Regeneración y Trasplante Cardíaco, Instituto de Investigación Sanitaria La Fe, Av. Fernando Abril Martorell Torre A, 46026, Valencia, Spain

[3]Departament d'Enginyeria Química. Escola Tècnica Superior d'Enginyeria. Universitat de València. Av. de la Universitat, s/n, 46100, Burjassot, Spain

[*]Corresponding author:

A. Ribes-Greus

aribes@ter.upv.es

Tel. 0034 630125695

Abstract

The endorsement of functional features such as biocompatibility, mechanical integrity, or electrical conductivity to tissue engineering (TE) scaffolds is essential to stimulate cell adhesion and proliferation. In this study, electrospun nanofibers based on polycaprolactone (PCL) and gelatin (Ge) (ratios 60/40, 50/50, and 40/60), and polyaniline (PAni) particles (0.25, 0.50, and 1.00 %wt) were prepared. The time of dissolution in an acid solvent mixture before electrospinning allowed for obtaining nanofibers with controlled features. Changes in the molar mass (M_n from $90{\cdot}10^3$ to $15{\cdot}10^3$ g·mol^{-1}), in the crystalline microstructure (X_c from 60 to 25%) and the surface morphology (diameter from 250 to 50 nm) due to the controlled hydrolytic action on PCL were found. *In vitro* degradability and biocompatibility were favoured as the dissolution time and gelatin percentage increased. The presence of PAni was revealed as non-cytotoxic and promoted a controlled increase of the electrical conductivity, that contributed to *in vitro* cardiomyocyte proliferation. Cellular centres in the vicinities of PAni microparticles could be identified in the scaffold with the 40/60 PCL/Ge scaffold with PAni (1.00 %wt), keeping the macrophages profile unaltered, which may determine the satisfactory resolution of cardiac injury and point out these scaffolds as appropriate candidates for cardiac TE.

Keywords

Tissue engineering, electrospinning, conductive scaffold, polycaprolactone (PCL), gelatin (Ge), polyaniline (PAni)

Graphical abstract

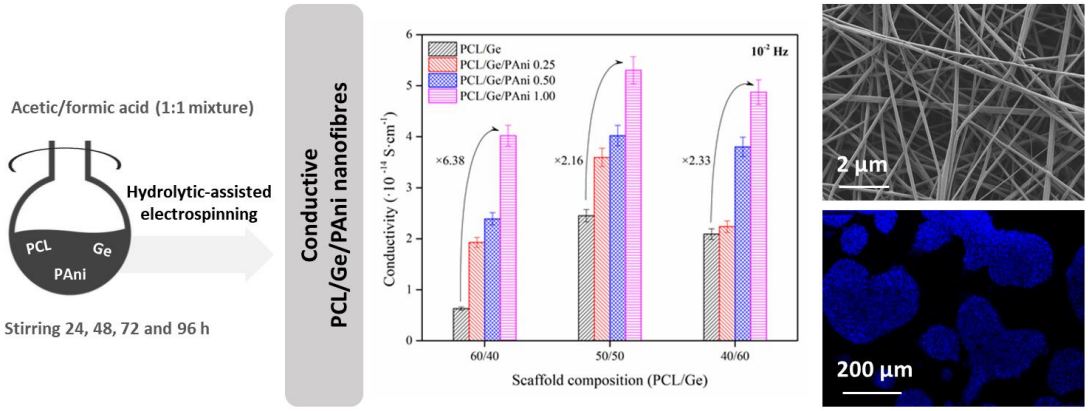

List of abbreviations

Acronym	Description
AA	Acetic acid
ATCC	American Type Culture Collection
ATR	Attenuated total reflectance
DAPI	4',6-diamidino-2-phyenylindole
DC	Direct Current
dn/dc	Refractive index increment
DSC	Differential scanning calorimetry
DT	Dissolution time
DTG	Derivative thermogravimetric curve
DTS	Dielectric thermal impedance spectroscopy
ECM	Extracellular matrix
FA	Formic acid
FBS	Foetal bovine serum
FE-SEM	Field-emission scanning electron microscopy
FT-IR	Fourier transform infrared spectroscopy
GAPDH	Glyceraldehyde-3-phosphate dehydrogenase
Ge	Gelatin
h_m	Melting enthalpy
LALS	Low angle light scattering
LDH	Lactate dehydrogenase
l_c	Lamellar thickness
M_n	Average molar mass in number
MTT	Methyl-thiazolyl-tetrazolium assay
M_w	Average molar mass in weight
PAni	Polyaniline
PBS	Phosphate buffered saline
PCL	Polycaprolactone
PCR	Polymerase chain reaction
PFA	Paraformaldehyde
PPy	Polypyrrole
PTFE	Polytetrafluoroethylene
RALS	Right angle light scattering
RGD	Arginylglycylaspartic acid
RPMI	Roswell Park Memorial Institute
SEC	Size exclusion chromatography
TE	Tissue engineering
TGA	Thermogravimetric analysis
THF	Tetrahydrofuran
T_m	Melting temperature
T_p	Peak temperature
X_c	Crystallinity degree
ρ	Density
σ_{elec}	Electrical conductivity
[η]	Intrinsic viscosity

1. Introduction

As an interdisciplinary field, tissue engineering (TE) considers three basic components to develop bio-functional substitutes for restoring tissue function: cells, biomaterials, and biomolecules. The application of biomaterials in TE is predominately in the form of scaffolds, which act as the temporary structure or physical guidance of the tissue to be formed. However, designing an ideal scaffold that mimics the structure and bio functions of the native extracellular matrix (ECM) is still a challenge. A suitable scaffold for TE should (*i*) provide a physical environment and bioactive components to support and stimulate the cell adhesion and tissue formation; (*ii*) offer mechanical strength similar to the tissue it temporarily replaces; (*iii*) allow the cells to restore the tissue architecture and be assimilated in a delimited time-span [1].

The combination of electrospinning and synthetic and natural polymers has brought new possibilities in the tissue regeneration field [2]. In this line, the development of novel electrospinning strategies for the production of functionalized scaffolds revealed promising results for biomedical applications. The preparation of polymer blends, copolymers or composites [3–6], the use of specific experimental setups for co-axial or tri-axial spinning [7] or random/aligned fibre collection [8], and the possibility of resorting to methods of chemical modification in solution are some of the existing approaches for obtaining electrospun functionalised scaffolds [9,10].

Among other possibilities, the use of biodegradable polyesters and the combination with natural polymers have gained great attention [11]. In particular, blending of polycaprolactone (PCL) and gelatin (Ge) through a hydrolytic-assisted method for tailoring the physicochemical features of the scaffolds resulted in nanofibers that combine high structural integrity as well as high *in vitro* and *in vivo* biocompatibility with low cost and high availability [12–14]. Whilst PCL has appropriate mechanical properties, biocompatibility, and slow biodegradability, the lack of hydrophilic functional groups in its structure requires its combination with hydrophilic and biocompatible materials [15–19]. Such is the case of Ge, which is composed of Arginyl-Glycyl-Aspartic amino acid sequences (RGD), that offer biochemical signals to promote cell adhesion, migration, proliferation, and differentiation [20]. In this regard, bicomponent PCL/Ge nanofibrous scaffolds have been proposed as a versatile substrate for the recovery of skin [21–24], muscle [25], cardiovascular [26,27], nerve [28,29], bone [30–33], and cartilage [34].

In some tissue engineering applications, the functionalisation of the scaffolds is essential to boost cell adhesion and proliferation [35]. In particular, there are tissues in which electrical stimuli play a key role during regeneration [36–42]. Some conductive synthetic polymers such as polyaniline (PAni) or polypyrrole (PPy) have been reported in the bibliography as good candidates for being used in the tissue

engineering field [43–47]. In such polymers with conjugated molecules, intrinsic charge carriers may be introduced in their structure, so that the bandgap is reduced and the system becomes conductive. This process is usually known as doping and it involves the formation of a polymer salt by exposing the polymer to the dopant in solution or by an electrochemical process. Doping allows electrons to flow due to the formation of conduction bands, that make the polymer conductive. As doping occurs, the electrons in conjugation can jump around the polymer chains. In particular, for PAni, the emeraldine salt conducting form is obtained from the modification of the insulating form emeraldine base, containing two amine nitrogen atoms followed by two imine nitrogen atoms [48]. These materials provide electrical conductivity to the scaffold when added in small amounts along with good biocompatibility and relatively easy assimilation by the human body [49]. However, when they are in excess, phase separation may occur, biodegradability and biocompatibility possibly will be concerned and toxicity and reduced cell viability can happen [50]. It must be also considered that, when combined with other hydrophilic polymers such as gelatin, that retain water molecules, electric conductivity will be boosted [51]. In the literature, several articles about the preparation of nanofibrous scaffolds, patches, and gels containing dispersed PAni microparticles or nanofibers in different biopolymer matrices have been reported, most of them with promising results in the tissue regeneration field [52–54].

The novelty of this work is the development of conductive polycaprolactone/gelatin/polyaniline nanofibres as functional scaffolds with tailored physicochemical properties using a hydrolytic-assisted electrospinning process, for bringing a suitable performance for cardiac tissue regeneration. Consequently, the aim of this study was, to obtain electrospun PCL/Ge/PAni scaffolds, and assess their behaviour under the blending, functionalization, and tailoring perspectives, as schematized in **Figure 1**. According to previous studies [13], balanced compositions of PCL and Ge of 60/40, 50/50, and 40/60 %wt were chosen. PAni content varying between 0.25 and 1.00 %wt, and dissolution time in 1:1 formic acid (FA) and acetic acid (AA) varying from 24 to 96 h were considered. The evaluation of the nanofibers was performed in terms of electrical conductivity, chemical structure, fibre morphology, thermal properties, and molar mass. As well, the evaluation of the *in vitro* behaviour of the scaffolds under simulated physiologic conditions and the study of the *in vitro* biocompatibility, cytotoxicity, and macrophage profiles were assessed.

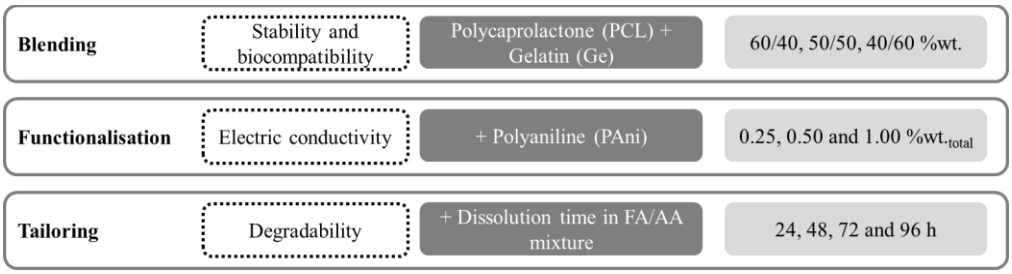

Figure 1. Scaffold preparation scheme according to the blending, functionalisation, and tailoring approach.

2. Materials and methods

2.1. Materials

Polycaprolactone (PCL) was provided by Sigma-Aldrich as 3 mm diameter pellets (M_n = 80000 g·mol^{-1}, T_m = 60 °C, ρ = 1.145 g·mL^{-1} at 25 °C). Gelatin (Ge) type A, derived from acid-cured porcine skin, was provided by Sigma-Aldrich, with solubility in H_2O at 50 mg·mL^{-1} and gel strength 300. Polyaniline (PAni) emeraldine salt was provided by Sigma-Aldrich as powder with average diameter 3-100 μm (M_w > 15000 g·mol^{-1}, conductivity 2-4 S·cm^{-1}, T_m > 300 °C, ρ = 1.360 g·mL^{-1} at 25 °C). Formic acid was provided by Scharlau (≥98%) (ρ = 1.220 g·mL^{-1}). Acetic acid (ρ = 1.050 g·mL^{-1}) was provided by Panreac (≥99%).

2.2. Polymer solution and electrospinning

The solutions for electrospinning were prepared in formic/acetic acid (1:1), with a polymer concentration of 15 %wt, with PCL and Ge weight proportions of 60/40, 50/50, and 40/60, respectively [13]. Subsequently, different weight percentages of PAni (0.25, 0.50, and 1.00 %wt) concerning the total solid concentration were added to the solutions, as shown in **Table 1**. Solutions were stored in an oven at 30 °C under magnetic stirring and were electrospun after 24, 48, 72, and 96 h of dissolution time.

Given the insolubility of the PAni microparticles in the selected solvent mixture along with the hydrolytic degradation of the PCL molecules, high PAni concentrations would result in the formation of aggregates and/or precipitation into the syringe during electrospinning, respectively. In this regard, the reduction of the solution viscosity during the different stages defined from 24 to 96 h under stirring at 30 ºC before electrospinning would result in lower entanglement capability of the PCL fraction and subsequent lower entrapment ability to hold PAni microparticles. The reduction of the intrinsic viscosity ([η]) of the PCL fraction as a function of dissolution time is shown in **Figure S1** in the Supporting Information. Although intrinsic viscosity of the PCL was significantly reduced, the presence of Ge helped to hold the PAni particles in the suspensions. Indeed, dissolutions remained reasonably stable under static conditions up to 60 min, necessary for the steady-state electrospinning. As a visual example, **Figure S2** shows the suspension stability of the 50/50 PCL/Ge compositions containing PAni after being stirred for 72 h at 30 ºC and left in static conditions resembling those into the syringe.

Table 1. Composition of the electrospun scaffolds for each dissolution time stage (24, 48, 72, and 96 h).

PCL (%wt)	Ge (%wt)	PAni (%wt$_{total}$)
60	40	-
		0.25
		0.50
		1.00
50	50	-
		0.25
		0.50
		1.00
40	60	-
		0.25
		0.50
		1.00

Electrospinning was performed in a horizontal compact lab-scale setup Bioinicia Fluidnatek® LE-10, which assembled a high voltage source, a programmable syringe pump, an HSW Norm-Ject 20 mL Luer Lock syringe, connected to a gauge 21 metallic needle employing Teflon® tubing and a grounded flat collector. The tip-to-collector distance was maintained constant at 17 cm. The voltage and the flow rate varied from 0.7 to 1 mL·h^{-1} and 19 to 25 kV respectively, to establish a steady-state condition. To obtain scaffolds with similar consistence, 4 mL of solution were electrospun in all cases. According to the perceived solution stability, the dissolution was magnetically stirred into the syringe every 30 min during electrospinning. The nanofibrous scaffolds were collected onto waxed paper and the residual solvent was allowed to evaporate at room temperature for 2 h, before storing them into zip bags for further analyses. The electrospinning process was performed at 22 ºC and 35% of relative humidity. All the samples showed a smooth surface with a circular shape of 10 cm in diameter.

2.3. Physico-chemical characterisation

2.3.1. Dielectric thermal impedance spectroscopy (DTS)

The impedance measurements were performed using a Novocontrol Broadband Dielectric Impedance Spectrometer (BDIS) connected with a Novocontrol Alpha-A Frequency Response Analyser. A BDS-1200 Novocontrol parallel-plated capacitor with two plated electrodes system was used as a dielectric cell test. The thicknesses of the scaffolds were evaluated using a micrometre Mitutoyo Comparator Stand 215-611 BS-10M taking the average of six measurements in different positions of the sample. The analyses consisted of a single sweep at room temperature (25±1 °C) in a frequency range from 10^{-2} to 10^{7} Hz. The electrical conductivity (σ_{elec}) was measured at low frequencies, where the measured real part of the conductivity (σ') reaches a plateau that is correlated to the direct current (DC) conductivity (σ_0).

2.3.2. Fourier transform infrared spectroscopy (FT-IR)

The scaffold composition was analysed using Fourier transform infrared spectroscopy (FT-IR) in a Thermo Nicolet ™ 5700 FT-IR equipment, coupled with an attenuated reflectance (ATR) module for measuring solid samples. The IR spectrum was obtained in the range from 4000 cm^{-1} to 400 cm^{-1}, with a resolution of 4 cm^{-1}, over 64 scans. Initially, the background was analysed. Then, up to five measurements were made from different points of the sample and the average spectra were taken as representative.

2.3.3. Thermogravimetric analysis (TGA)

The presence of the different components of the scaffold was indirectly analysed utilizing thermo-oxidative decomposition behaviour in a Mettler-Toledo TGA 851 thermogravimetric analyser. The samples, with a mass between 3 and 5 mg, were introduced into 70 μL alumina crucibles. They were then subjected to a dynamic assay, based on a heating segment from 25 ºC to 800 ºC with a heating rate of 10 $ºC \cdot min^{-1}$. The analyses were carried out under an oxidative atmosphere with a feeding rate of oxygen of 50 $mL \cdot min^{-1}$. The samples were studied in triplicates and the averages of results were taken as representative.

2.3.4. Field-emission scanning electron microscopy (FE-SEM)

The surface topology of the scaffolds was analysed by a field emission scanning electron microscope (FE-SEM) model Zeiss Ultra 55. The samples were coated in a Leica EM MED020 sputter coater to create a metallic layer of platinum during 10 s under an inert atmosphere and vacuum conditions. Once the samples were coated, they were placed onto the sample holders and introduced into the FE-SEM equipment. The micrographs were taken using a working distance between 4 to 5 mm, a voltage of 1 kV, and a magnification of 10000×. The diameter of the nanofibers was measured from the average of random locations (*n=100*) with the aid of the software Image J®.

2.3.5. Differential scanning calorimetry (DSC)

The crystalline structure was analysed from a calorimetric perspective, using a Mettler-Toledo DSC 820^e differential scanning calorimeter. The samples, with a mass of around 5 mg, were introduced into 40 μL aluminium crucibles perforated on top. The method of analysis consisted of a heating scan between 10 ºC and 120 ºC with a rate of 10 $ºC \cdot min^{-1}$. The test was carried out under an inert nitrogen atmosphere with a flow rate of 50 $mL \cdot min^{-1}$. The samples were analysed in triplicates and the averages of results were taken as representative.

The crystallinity degree (X_c) was evaluated from the melting enthalpy results, using **Equation 1**,

$$X_c\ (\%) = \frac{1}{w_{PCL}} \cdot \frac{\Delta h_m}{\Delta h_m^0} \cdot 100 \qquad (1)$$

where w_{PCL} is the weight percentage of the PCL in the scaffold, Δh_m is the analysed melting enthalpy and $\Delta h_m{}^0$ is the melting enthalpy of a perfect crystal of PCL (148 J·g^{-1}) [55].

The lamellar thickness (l_c) was calculated by applying the Thomson-Gibbs equation (**Equation 2**), based on the temperatures associated with the peak of the melting transitions [56–59],

$$l_c(T_m) = \left[\left(1 - \frac{T_m}{T_m^0}\right) \cdot \frac{\Delta h_{mv}}{2 \cdot \sigma_e}\right]^{-1} \qquad (2)$$

where T_m is the melting temperature; $T_m{}^0$ is the equilibrium melting temperature of an infinite crystal (348 K), σ_e is the surface free energy of the basal plane where the chains fold (106·10^{-3} J·m^{-2}) and Δh_{mv} is the melting enthalpy per volume unit (1.63·10^8 J·m^{-3}) of PCL [60].

2.3.6. Size exclusion chromatography (SEC)

The molar mass was assessed through size exclusion chromatography (SEC) in a Malvern Instruments Omnisec Resolve chromatograph, which combined an integrated pump, a degasser, an autosampler, and a column oven, along with a Malvern Instruments Omnisec Reveal multi-detector –Ultraviolet (UV), Refractive Index (RI), Low and Right-Angle Light Scattering (LALS and RALS) and Viscosity (VISC)–. Two columns from Malvern Instruments (T2000 and T4000) were considered (300×8 mm). Tetrahydrofuran (THF) was used as a mobile phase at a flow rate of 1 mL·min^{-1} and column temperature of 35 ºC. The samples were dissolved in THF at concentrations of ~2.0 mg·ml^{-1} and were filtered through 0.45 µm polytetrafluoroethylene (PTFE) filters. For calibration, a monodisperse polystyrene standard with a dn/dc value of 0.185 was used. Two replicates per sample were performed and the obtained data were analysed with the aid of the Omnisec V10™ software.

2.4. In vitro validation

2.4.1. Degradation in simulated physiologic conditions

The scaffolds were subjected to hydrolytic degradation in phosphate buffer solution (PBS), according to the international standard ISO 10993-13:2010, method 4.3 [61]. The initial electrospun scaffolds were cut into rectangular specimens with a mass of around 10 mg. The specimens were weighed (m_0) and placed in a previously weighed vial (m_{vial}). 10 mL of degradation medium were introduced and then the vials were sealed with PTFE threaded plugs and placed in a thermostatically controlled oven at 37 ºC. The pH of the PBS solution was adjusted to 7.4 with NaOH 1 M. The effects of the hydrolytic degradation were evaluated after 100 days of immersion. Then, the scaffolds followed a washing-drying-keeping procedure.

Accordingly, samples were dried under vacuum to constant mass into their degradation vials (m_{dry}) and saved for further analyses. The mass variation of the specimens was calculated according to **Equation 3**.

$$Remaining\ mass\ (\%) = \frac{m_{dry} - m_{vial}}{m_0} \cdot 100 \qquad (3)$$

2.4.2. Biocompatibility

HL-1 cardiac muscle cell line was used to analyse the cellular adhesion and proliferation. Cells were cultured in a Claycomb medium (Sigma-Aldrich) supplemented with 10% foetal bovine serum (FBS, Gibco), 2 mM L-Glutamine, and 100 U·ml^{-1} – 100 µg·ml^{-1} Penicillin-streptomycin (P/S). Afterwards, 40000 cells were seeded onto 1 cm^2 of the scaffolds in triplicates, as previously described [13,62]. Subsequently, cells were fixed with 2% paraformaldehyde (PFA) after 48 and 96 h, and cellular nuclei were stained with 4',6-diamidino-2-phenylindole (DAPI). Images were acquired through a Leica DM2500 fluorescence microscope. To evaluate the cellular viability, the thiazolyl blue tetrazolium bromide assay (MTT, Sigma-Aldrich) was carried out after 48 and 96 h, following the manufacturer's recommendations. Absorbance was measured at 550 nm using a plate reader HaLo Led 96 (Dynamica Scientific Ltd.) and proliferation was evaluated as the ratio of MTT values obtained at 96 h/48 h. Experiments were carried out in triplicates of three independent experiments and the averages were considered representative.

2.4.3. Lactate dehydrogenase activity assay

The lactate dehydrogenase (LDH) activity released from HL-1 Cells seeded onto the scaffolds into the medium was tested using the LDH cytotoxicity detection kit (Merck). Briefly, cells were seeded as described in the previous section and, after 48 h, supernatants were transferred to a 96 well plate and incubated with specific reagents and protected from light for 30 min at 25 ºC. Then, absorbance was measured at 494 nm using the HaLo Led 96 (Dynamica Scientific Ltd.) plate reader. For normalization, total protein was extracted from cells and quantified with the Pierce™ BCA Protein Assay Kit (Thermo Scientific). Experiments were performed in triplicates of three independent experiments and the averages were considered representative.

2.4.4. Macrophage M1 and M2 profile

THP-1 Cells from the American Type Culture Collection (ATCC) were cultured in Roswell Park Memorial Institute (RPMI) medium supplemented with 10% FBS and were stimulated into the M0, M1, and M2 phenotypes as described by Graney *et al.* [63]. Briefly, 200000 cells were seeded onto the scaffolds in triplicates and were treated for 24 h with 200 ng·ml^{-1} phorbol 12-myristate-13-acetate to differentiate to M0. Then cells were incubated for 48 h in 100 ng·ml^{-1} lipopolysaccharide and 100 ng·ml^{-1} interferon-ɣ (M1) or 40 ng·ml^{-1} interleukin-4 (M2). Afterwards, RNA was isolated using an RNeasy Plus

kit (Qiagen). cDNA was produced using PrimeScriptTM RT Reagent kit (Takara Bio), and real-time polymerase chain reaction (qPCR) was performed using TB Green® Premix Ex TaqTM (Takara Bio) on a ViiA 7 Real-Time PCR System (ThermoFisher Scientific). Primers were provided by Condalab, and glyceraldehyde-3-phosphate dehydrogenase (GAPDH) was used as a reference gene. Experiments were performed in triplicates of three independent experiments and the averages were considered representative.

2.4.5. Statistical analyses for the biological validation

Data are represented as mean ± standard deviation (SD). Statistical analyses were carried out using GraphPad Prism 8® software. Statistical significance was determined with the non-parametric one or two-way ANOVA and appropriate post hoc analysis. Differences were considered statistically significant at $p < 0.05$ with a 95% confidence interval.

3. Results and discussion

The produced PCL/Ge/PAni nanofibres were evaluated in terms of electrical conductivity, chemical structure, morphology and dimensions, crystalline structure, and molar mass. As well, the *in vitro* degradation in simulated physiologic conditions was assessed and the *in vitro* biocompatibility was analysed in terms of cell proliferation, lactate dehydrogenase assay, and macrophage profile.

3.1. Electrical conductivity

The functionalisation of the scaffolds as a result of the addition of polyaniline (PAni) was evaluated through dielectric thermal impedance spectroscopy (DTS) and the electrical conductivity *(σ_{elec})* was calculated. The obtained σ_{elec} *values measured at low frequencies (10^{-2} Hz) are plotted in* ***Figure 2***.

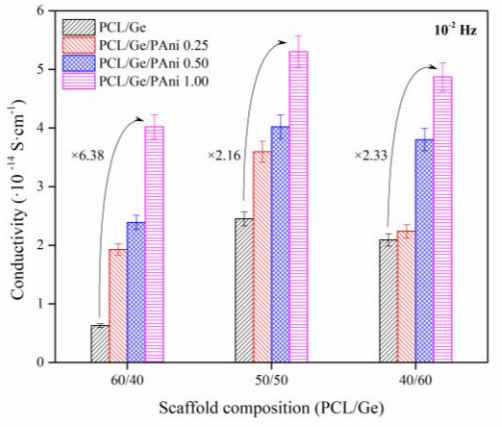

Figure 2*. Electrical conductivity (σ_{elec}) of the scaffolds as a function of the PCL/Ge composition and the PAni content.*

In general, even with the low content of PAni (≤1.00 %wt), a significant increase in the electrical conductivity of the nanofibres was perceived [47]. Although the obtained values were below the electrical conductivity of pure PAni, around 2-4 $S \cdot cm^{-1}$, *a substantial increase of the* σ_{elec} *was found in the scaffolds containing PAni microparticles. In particular, for the 60/40 composition, the electrical conductivity increased by 6.38 in comparison with plain PCL/Ge with the addition of PAni (1.00 %wt). As the Ge content augmented, the increase in the electric conductivity was less intense, and values higher than the double were found (×2.16 and ×2.33) for the 50/50 and 40/60 PCL/Ge compositions. The contribution of water molecules retained in the Ge structure along with its intrinsic polyampholyte character may promote this higher conductivity in compositions with a high Ge percentage [64]. Altogether, these results corroborated the presence of PAni in the scaffolds and validated the functionalisation strategy for increasing the electrical conductivity of the nanofibres for electrical-stimulated cell growth applications [48].*

3.2. Structure and composition

The combination of polycaprolactone (PCL), gelatin (Ge), and polyaniline (PAni) in different percentages may result in functional scaffolds with dissimilar structures. Moreover, the effect of the dissolution time may promote differences in the chemical structure of the nanofibres. Therefore, the evaluation of both the presence of characteristic functional groups as well as the composition is of great importance for the chemical identification and compatibility evaluation, respectively [65–69]. In this regard, Fourier-transformed infrared spectroscopy and thermogravimetric analyses were carried out. As an illustrative example, the results obtained for the nanofibres electrospun after 24 h of dissolution time are shown in this section. The observed tendencies applied to the other dissolution times.

In terms of composition, the FT-IR spectra of the PCL/Ge scaffolds (60/40, 50/50, and 40/60) as a function of the PAni content were analysed and *plotted in* ***Figure 3****. The pure* PCL has the main absorption bands at 1727 cm^{-1}, associated with C═O stretching vibration in carbonyl groups, 2865 cm^{-1} correlated to the symmetric CH_2 stretching, and 2950 cm^{-1} due to the asymmetric CH_2 stretching [70]. The pure Ge reveals the peaks at 1627 cm^{-1} for amide I, 1540 cm^{-1} for amide II, and 3300 cm^{-1} for amide A bands [71]. These signals are mainly correlated to the stretching vibrations of C═O bonds, the coupling of the bending of N─H and the stretching of C─N bonds, and the N─H stretching vibration, respectively [70]. The pure PAni spectrum shows its main bands in the region of 1551, 1445, and 1286 cm^{-1}, corresponding to the ring-stretching vibrations of the quinoid and benzenoid rings of aniline and nitro aniline, respectively [45]. As well, the bands at 2916 and the 780 cm^{-1} correspond to the vibration of the C−H aromatic ring and the C−H in-plane bending vibration [72].

The characteristic peaks of both the PCL and the Ge molecules were represented in the spectra of the obtained nanofibres, in which the intensity of the peaks varied as a function of the composition of the scaffold [65]. Moreover, a slight shift of the carbonyl group of the ester bond towards a higher wavelength (1720 in PCL to 1724 cm^{-1} in the blends) may suggest hydrogen-bonding interactions between both components. In general, the peaks associated with the PAni were absent for all the compositions. This observation may be correlated to the low concentration of the PAni particles *(≤1.00 %wt)* along with a good dispersion into the PCL/Ge matrix. Moreover, given the similarities in the wavelength of the bands, the characteristic PAni peaks may have been overlapped by the more intense bands of the PCL and Ge.

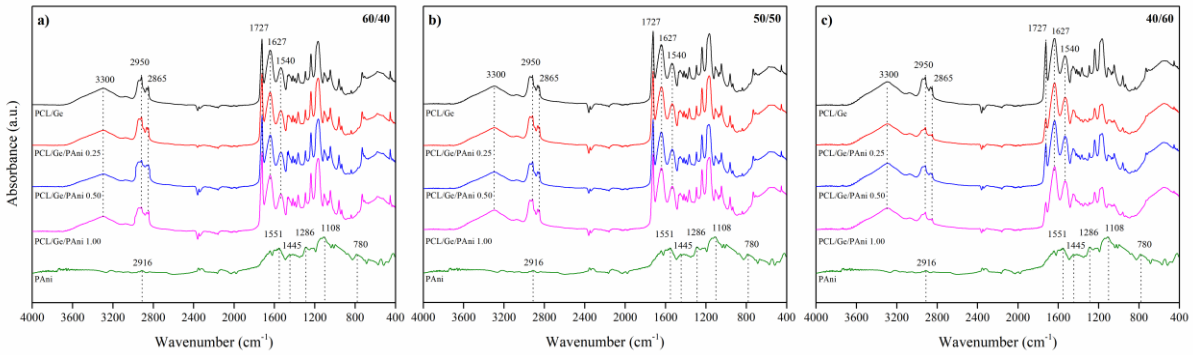

***Figure 3**. Stacked FTIR spectra of the scaffolds as a function of PCL/Ge proportion and the PAni content* for a dissolution time of 24 h. *Plots are labelled according to the PCL/Ge composition as a) 60/40; b) 50/50; and c) 40/60.*

Afterwards, the evaluation of the thermo-oxidative stability was considered as a useful approach for assessing the composition of the scaffolds through the stages for the thermal decomposition of the different components. The stacked thermo-gravimetric and first derivative thermo-gravimetric curves (DTG) of the PCL/Ge scaffolds (60/40, 50/50, and 40/60) as a function of the PAni content are plotted in **Figure 4**. The decomposition stages were furtherly characterised in terms of peak temperatures (T_p) and mass-loss (Δm), which are gathered in **Table 2**. ***Figures S3** and **S4** in the Supplementary Material show the thermogravimetric and DTG curves as a function of the PAni content for further dissolution time.*

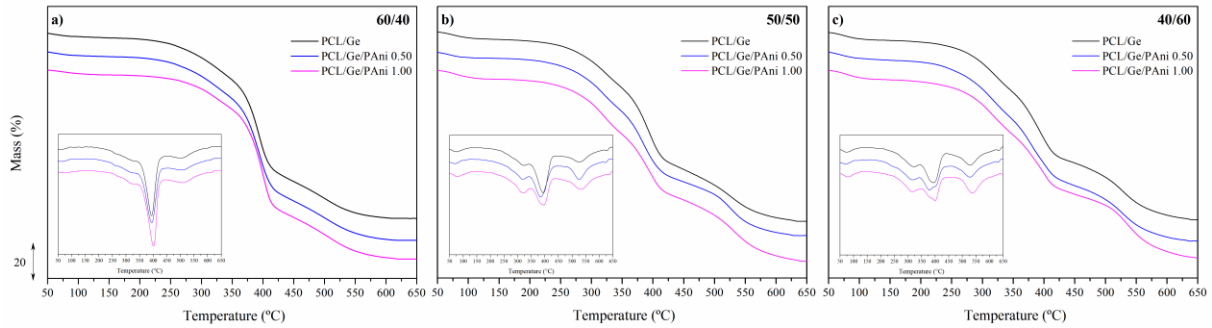

Figure 4. *Stacked thermo-gravimetric and first derivative thermo-gravimetric curves (DTG) (inset)* of the scaffolds *as a function of PCL/Ge proportion and the PAni content* for a dissolution time of 24 h. *Plots are labelled according to the PCL/Ge composition as a) 60/40; b) 50/50; and c) 40/60.*

Table 2. Mass loss percentage (Δm) and peak temperature (T_p) of the different thermo-oxidative decomposition stages as a function of the scaffold composition for a dissolution time of 24 h.

		Stage 1		**Stage 2**		**Stage 3**		**Stage 4**		**Res.**
PCL/Ge	**PAni**	Δm_1	T_{p1}	Δm_2	T_{p2}	Δm_3	T_{p3}	Δm_4	T_{p4}	***R***
(%)	**(%)**	**(%)**	**(°C)**	**(%)**	**(°C)**	**(%)**	**(°C)**	**(%)**	**(°C)**	**(%)**
60/40	-	4.14	55.94	18.86	327.13	56.68	393.61	20.03	503.09	0.29
	0.50	3.59	59.81	18.66	321.41	56.16	394.19	21.38	504.27	0.21
	1.00	3.07	75.71	18.57	318.09	56.35	400.55	21.36	507.70	0.65
50/50	-	4.30	74.73	23.66	323.57	43.76	393.91	27.63	527.23	0.65
	0.50	4.33	72.80	26.19	320.01	39.67	391.21	28.79	527.12	1.02
	1.00	5.32	79.37	29.00	321.38	33.48	394.06	31.67	531.03	0.53
40/60	-	4.90	73.95	25.00	323.03	40.11	394.67	29.45	528.32	0.54
	0.50	5.25	72.18	28.55	315.95	37.90	400.13	27.49	528.06	0.81
	1.00	5.67	75.95	28.70	315.74	34.08	399.62	31.30	537.54	0.25

The pure PCL possesses two-stage decomposition, while the pure Ge has three mass-loss stages [14]. The PCL/Ge/PAni scaffolds showed an intermediate behaviour in which the contributions to the different stages were related to the PCL and Ge proportions. Although incomplete miscibility was reported for the PCL/Ge system [73], according to the obtained results they may be classified as compatible, an intermediate state between miscibility and immiscibility in which they exhibit macroscopically uniform properties.

The evaluation of the mass loss curves of the PCL/Ge/PAni scaffolds showed the first stage from 50 to 150 ºC due to the evaporation of moisture [74,75]. Indeed, as the Ge content increased in the blend, a higher contribution to this stage was found. Particularly, water content grew up to 6% in the scaffolds with the higher content of Ge. Stage 2 from 250 to 350 °C may be ascribed to a complex decomposition

process including protein chain breakage and peptide bond rupture of the Ge molecules [74]. Next, the thermo-oxidative degradation of the PCL backbone was found, defined as stage 3, and was partially overlapped with stage 2 in the range from 300 to 450 ºC. Finally, stage 4 involved the thermo-oxidative degradation of the previously formed residues from 450 ºC onwards. Given the overlapped behaviour of the decomposition reactions, a direct assignation of each stage to a given component may not be assumed. However, the progressive perceived pattern, especially in the mass loss of stages gathered in **Table 2**, may suggest an appropriate blending strategy. The contribution of the PAni could be perceived in the higher moisture release temperature, especially for the 60/40 PCL/Ge scaffolds with PAni (1.00 %wt), which may be ascribed to stronger scaffold-water interactions. Moreover, it slightly moved the decomposition temperatures of stages 3 and 4 towards higher values. This behaviour could be correlated to the superior thermal stability of PAni, in which backbone decomposition occurs above 300 ºC and up to 650 ºC [76,77]. Finally, a decomposition residue was found below 1% in all the samples, which corroborates the complete thermo-oxidation of the scaffolds at the end of the assay.

3.3. Nanofibrous morphology, crystalline structure, and molar mass

In this section, the variations of the nanofibrous morphology, the crystalline structure, and the molar mass of the PCL fraction were assessed for the different compositions and dissolution times.

The morphology of the electrospun nanofibres is known to play a key role during application. For satisfactory cell attachment and proliferation, nanofibres must mimic the extra-cellular matrix in size and structure [78]. Therefore, the surface of the scaffolds was studied through field-emission scanning electron microscopy (FE-SEM). The obtained electron micrographs are shown in **Figure 5**. Moreover, the nanofibre diameter was evaluated, which results are shown in **Figure S5** and **Figure 6** as histograms and average values, respectively

The fibre diameter was found in the nanometric scale for all the compositions. Indeed, although the diameter increased as a function of the Ge content, the average size was always below 300 nm. A higher percentage of Ge in the blends has been reported in the literature to promote higher solution conductivity and lower viscosity, and subsequently lower fibre diameter after electrospinning [79,80]. However, the higher diameter found in the produced nanofibres in this study when Ge content increased may be due to their flat ribbon-like shape instead of circular fibre cross-sections [81]. This flat morphology may have been produced as a consequence of the impact of the wet electrospinning jet with the collector, causing the flattening of the fibres that resulted in greater diameter. The presence of remnant solvent in the jet during collection may have contributed to produce flatted shapes instead of fibres with a purely circular cross-section. Complementarily, after spinning, the solvent contained in the fibres diffuses out into the

atmosphere, and the resulting barometric pressure may distort the cylindrical fibres to the perceived flat morphology [82].

The effect of the addition of PAni was insignificant in terms of the average fibre diameter. Although the addition of PAni could have increased the conductivity of the electrospinning solution and therefore result in lower fibre diameter, a clear effect was not perceived. These observations can be due to the low amounts of PAni (≤1.00 %wt), along with a relatively low total solid concentration of the electrospinning solutions (~15 %wt), and suitable dispersion of the PAni particles into the PCL/Ge mixture.

In agreement with previous studies [12,14], significant variations were found in the fibre diameter of the scaffolds as a function of the dissolution time for all the compositions. Thinner and more homogeneous fibres were found as dissolution time increased. Particularly, fibre diameter distributions became narrower and were significantly displaced to dimensions in the actual nanoscale range (<100 nm). In general, bead-free fibrous structures were obtained for the scaffolds prepared up to 72 h of dissolution in the acid solvent system. The hydrolytic degradation of the ester bonds of the PCL macromolecular chains, when diluted into the 1:1 formic/acetic acid mixture, reduced the solution viscosities, which caused a lower fibre diameter. Therefore, the control of the dissolution time before electrospinning stands out as a reliable parameter to tailor the dimensions of PCL/Ge/PAni scaffolds.

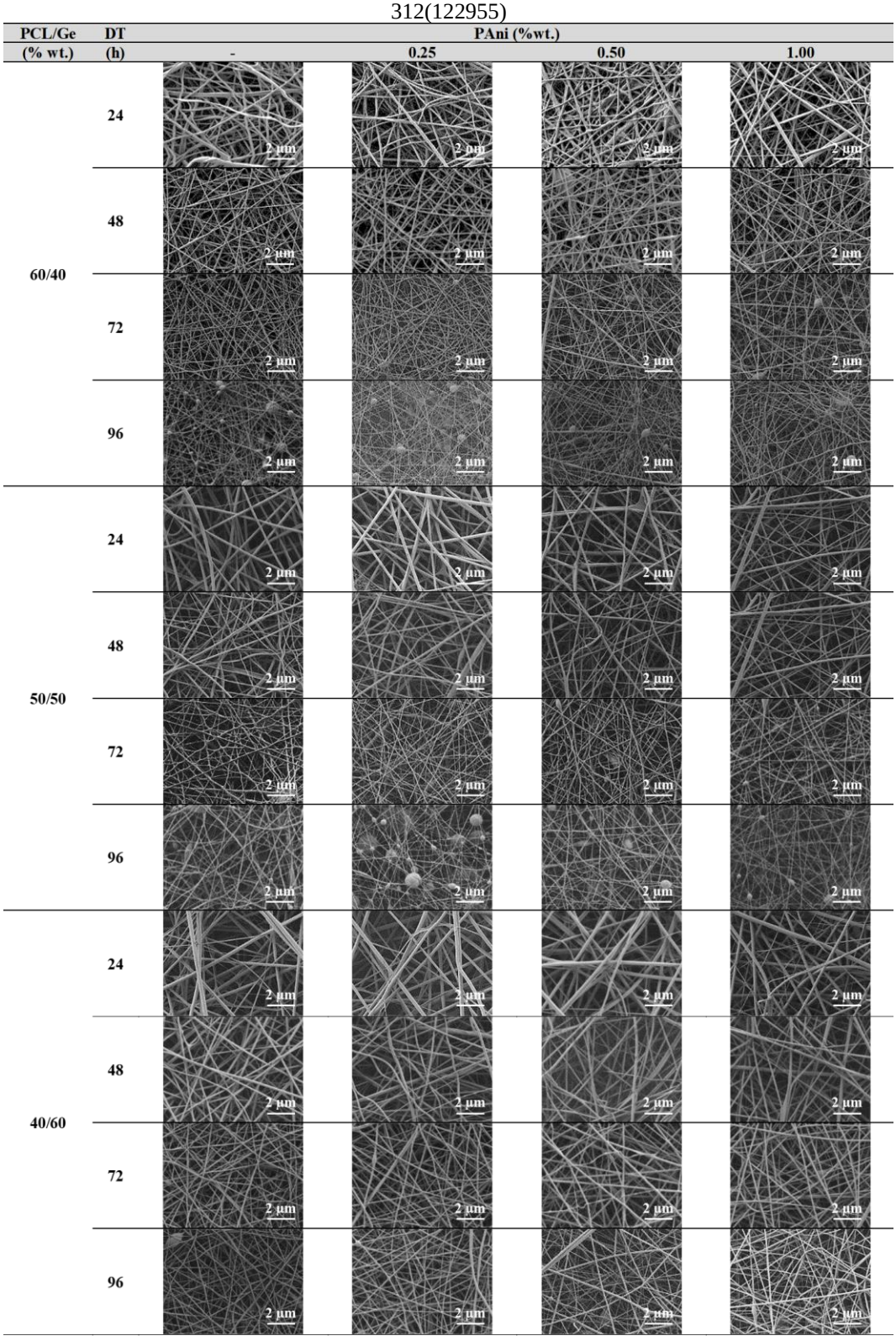

Figure 5. Surface morphology of the scaffolds as a function of the PCL/Ge composition, the PAni content, and the dissolution time (DT) (10000×).

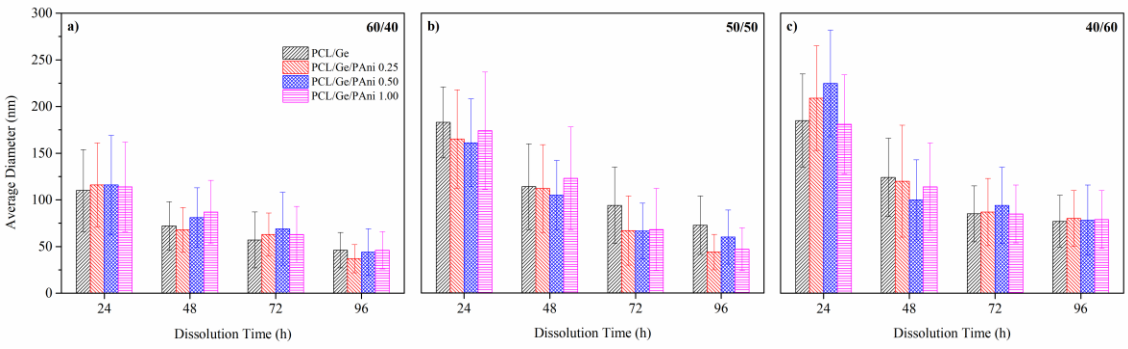

Figure 6. Average nanofibre diameter as a function of PCL/Ge proportion, the PAni content and the dissolution time. Plots are labelled according to the PCL/Ge composition as a) 60/40; b) 50/50; and c) 40/60.

The structure of the scaffolds was furtherly assessed and the thermal properties and crystallinity were analysed through differential scanning calorimetry (DSC). The first heating calorimetric thermograms of the PCL/Ge scaffolds (60/40, 50/50 and 40/60) as a function of the PAni content (0.50 and 1.00 %wt) and dissolution time are plotted in **Figure 7**.

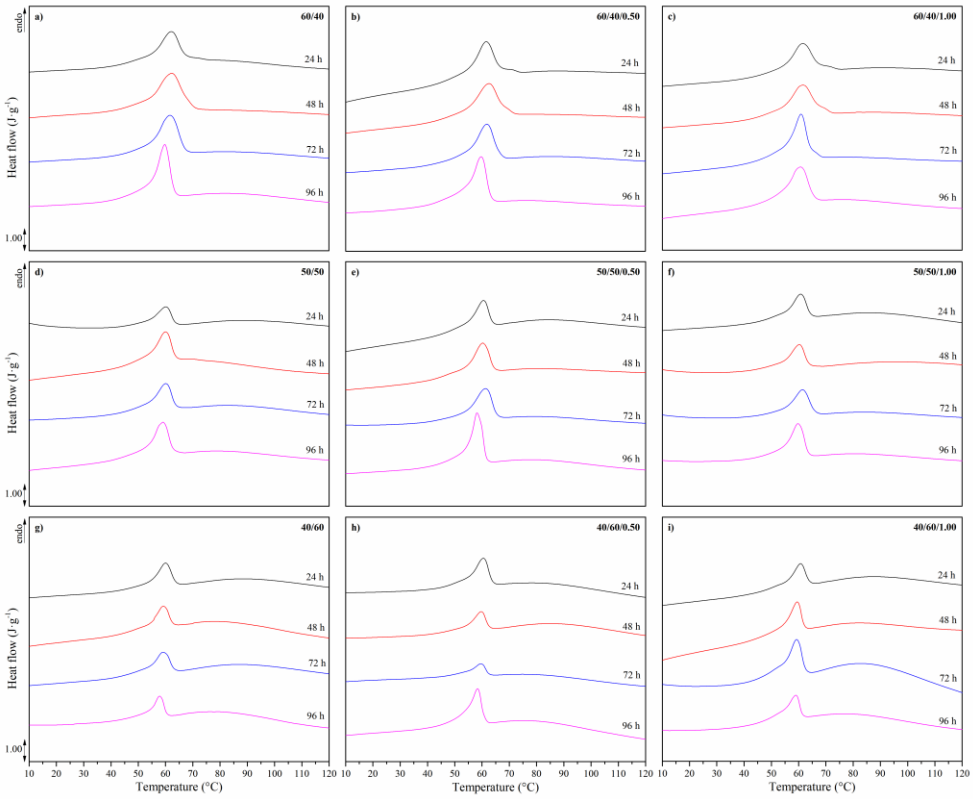

Figure 7. Stacked calorimetric thermograms of the first heating scan as a function of PCL/Ge proportion, the PAni content and the dissolution time. Plots are labelled according to the PCL/Ge/PAni composition as a) 60/40; b) 60/40/0.50; c) 60/40/1.00; d) 50/50; e) 50/50/0.50 ; f) 50/50/1.00 ; g) 40/60; h) 40/60/0.50; i) 40/60/1.00.

Slight differences were perceived as a function of the PCL/Ge composition (60/40, 50/50 and 40/60), correlated to the prevalence of each component in the blend, as perceived in previous sections. The endothermic melting peak of the PCL between 50 and 65 ºC moved towards lower temperatures and the melting enthalpy decreased for higher Ge proportion. Moreover, a wide transition from 30 to 110 ºC due to the release of moisture gained importance as the Ge content increased, highlighting its hydrophilic behaviour [14]. Some studies in the literature dealing with gelatin reported the characteristic helix to coil transition in the vicinities of 35 ºC [30,83]. However, this transition was absent in the obtained thermograms [84]. The denaturalisation of the helix conformation may have occurred during the dissolution of the Ge into the formic/acetic acid mixture.

The contribution of the PAni was not perceivable in the thermograms. Although slight modification of thermal transitions was perceived in other studies dealing with crosslinked Ge nanofibres with a proportion of PAni varying from 15 to 45 %wt [52], the low percentage considered in this study (<1.00 %wt) may not be high enough to alter the thermal transitions of the scaffolds.

Considering the dissolution time, while the wide endotherm of Ge remained unaltered, the melting peak of the PCL was sharpened and displaced towards lower temperatures for longer dissolution. As the PCL melting transition is strictly related to its crystalline structure, the reduction of the length of macromolecular PCL segments due to the hydrolytic chain scission during dissolution may have affected the resultant amorphous-to-crystalline ratio of the nanofibres [85–87]. From an application perspective, amorphous regions are predominantly hydrophilic, labile to hydrolytic degradation and therefore more biocompatible. Nevertheless, although the crystalline domains with a highly ordered and compact structure bring mechanical support, they are less permeable to water molecules and therefore more resistant to hydrolytic degradation and with less biological compatibility [88]. Therefore, the evaluation of the crystalline structure is crucial to infer the future biodegradation and bioassimilation performance as well as biocompatibility of the scaffolds during application [89].

Given the amorphous structure of the Ge, the crystallinity degree (X_c) and the lamellar thickness (l_c) of the PCL fraction were evaluated. These indicators have been previously proposed for monitoring the service behaviour of some biopolymers [90,91]. Consequently, the obtained results of the X_c are plotted in **Figure 8** and l_c is gathered in **Table 3**.

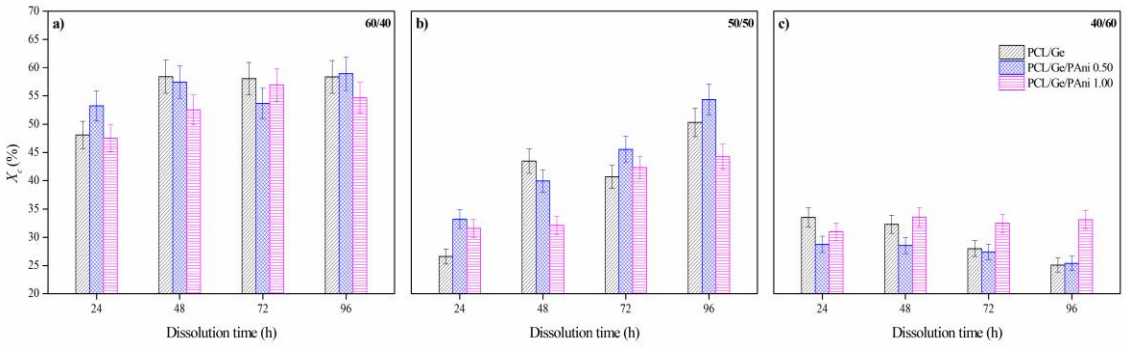

Figure 8. Crystallinity degree (X_c) of the PCL fraction as a function of PCL/Ge proportion, the PAni content, and the dissolution time. Plots are labelled according to the PCL/Ge composition as a) 60/40; b) 50/50; and c) 40/60.

Table 3. Lamellar thickness (l_c) in nm of the PCL fraction of the scaffolds as a function of PCL/Ge proportion, the PAni content, and the dissolution time. A standard deviation between 1 and 5% was omitted for the sake of clarity.

PCL/Ge	PAni	Dissolution time (h)			
(%wt)	(%wt)	24	48	72	96
60/40	-	34.87	35.22	33.93	29.88
	0.50	33.40	36.21	34.42	29.64
	1.00	33.11	33.48	32.05	31.70
50/50	-	29.99	29.99	29.97	28.39
	0.50	30.96	30.64	32.24	26.89
	1.00	33.09	30.96	30.09	29.72
40/60	-	29.93	28.43	28.39	26.59
	0.50	31.04	29.37	29.30	27.25
	1.00	31.30	29.00	28.74	28.18

The differences in the crystalline fraction due to the PCL-to-Ge proportion in the blends were significant, regardless of the content of PAni. *As the Ge content increased, the crystallisation of PCL was hindered and the crystallinity degree (X_c) significantly decreased from 50 to 35% for the 60/40 to the 40/60 composition*. Besides, the reduction of crystallinity was accompanied by a crystalline structure with a lower lamellar thickness (l_c) as the Ge content increased, moving from ~35 nm to ~29 nm from the 60/40 to the 40/60 composition *[73]*. *T*he presumable diffusion of the PCL macromolecules into the Ge matrix may have hindered the PCL crystallisation and resulted in the generation of crystalline domains with lower l_c [14].

The potential of the control of the dissolution time to tailor the crystalline morphology of the nanofibres was corroborated in terms of the percentage and size of the crystalline population. On the one hand,

scaffolds with 60/40 and 50/50 compositions showed an increasing tendency of the X_c due to the hydrolytic degradation of the PCL chains. Shorter macromolecular segments with enhanced mobility were more capable of forming crystalline domains than longer segments [17]. However, with a higher proportion of Ge in the 40/60 PCL/Ge scaffolds, the above-perceived crystallisation behaviour was altered. In this composition, the dissimilar and hydrolysed short PCL segments may have completely diffused into the Ge phase, which prevented the PCL from substantial crystallisation. Regarding the lamellar thickness, although dissimilarities were found for shorter dissolution times, it generally decreased as hydrolytic degradation progressed. This performance may be also ascribed to the generation of thinner crystalline structures composed of shorter hydrolysed polymer chains, which would result in higher biocompatibility and quicker bioassimilation periods.

Afterwards, the crystalline structure was correlated to the molar mass of the PCL fraction. For this purpose, size exclusion chromatography (SEC) was conducted, which results in terms of the average molar mass in number (M_n) are plotted in **Figure 9**. The M_n of the virgin PCL pellet was included for comparison purposes.

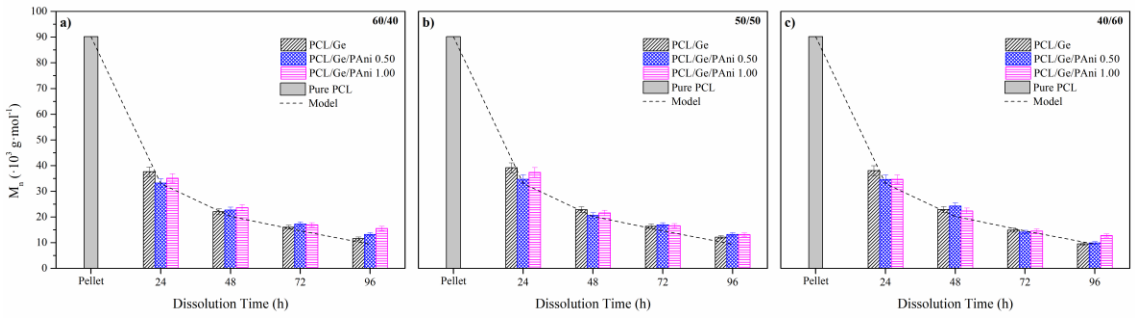

Figure 9. Average molar mass in number (M_n) of the PCL fraction in the 60/40, 50/50, and 40/60 PCL/Ge scaffolds as a function of the PAni content and the dissolution time. Plots are labelled according to the PCL/Ge composition as a) 60/40; b) 50/50; and c) 40/60.

In general, the hydrolytic degradation of the PCL during dissolution into the formic/acetic acid mixture was verified. Considering the molar mass of the PCL pellet before dissolution as M_n of $90 \cdot 10^3$ g·mol^{-1}, the PCL macromolecules were degraded faster at the early stage of the solution preparation and tended to decrease slowly thereafter [86,92]. This hydrolytic reaction may occur as a depolymerisation process and random chain scission mechanism, highly catalysed by the formic/acetic acid solution. Moreover, the ester bond breakage of the PCL molecules may result in the generation of new carboxylic ending groups, responsible for auto-catalytic degradation [93]. Results followed an exponential decreasing model as a function of the dissolution time, as proposed by Lavielle et al. [86] and corroborated in previous studies with pure PCL nanofibres [12]. It must be highlighted the proper correlation (>98% coincidence) between

the expected theoretical and experimental values regardless of the presence of Ge and PAni. Moreover, a linear correlation between the intrinsic viscosity ([η]) variation and the average molar mass in weight (M_w) of the PCL fraction was observed as dissolution time increased [86]. These results, plotted in **Figure S6** in the Supplementary Material, may allow for the intrinsic viscosity approximation as a function of the PCL molar mass, a parameter that significantly influences the fibre morphology after electrospinning.

Although hydrolysis and subsequent viscosity reduction of the Ge as a function of time when diluted in such acid solvent have been reported before [94], previous studies demonstrated that the addition of Ge to the blend contributed to retaining enough viscosity for suitable electrospinning [14]. This observation was also verified in this work in the micrographs shown in **Figure 5**, where more homogeneous nanofibres were obtained for higher dissolution time as Ge content increased. This phenomenon is particularly relevant for high dissolution times when the PCL molecules may be severely hydrolysed and the Ge molecules contribute to holding the molecule entanglements that allow for appropriate electrospinning.

Although other features such as the electrical conductivity, structure, and fibre morphology of the scaffolds changed due to the Ge and PAni contributions, as seen in previous sections, the tailoring approach for the molar mass modulation of the PCL fraction was not altered either by the presence of Ge or PAni.

3.4. In vitro degradation in simulated physiologic conditions

At this point, the long-term in vitro degradation of the electrospun PCL/Ge/PAni scaffolds was studied in simulated physiologic conditions through immersion in phosphate-buffered saline (PBS) medium during 100 days, under standardised conditions given by the ISO 10993-13:2010-method 4.3 [61,95]. The resulting variations of the mass and the pH of the degradation media are plotted in **Figure 10**.

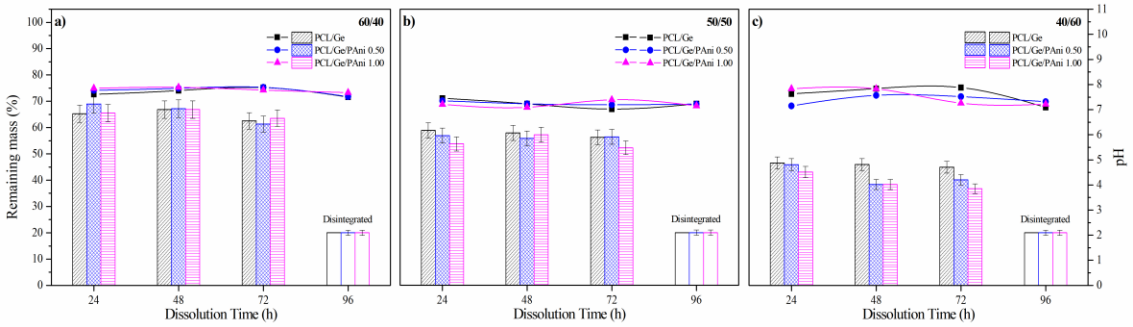

Figure 10. Relative mass variation (bars) of the scaffolds and pH (scatter) of the degradation media after 100 days in simulated physiological conditions (phosphate-buffered saline (PBS) at 37 ºC). Error bars (<3%) in pH results were omitted for the sake of clarity. Plots are labelled according to the PCL/Ge composition as a) 60/40; b) 50/50; and c) 40/60.

The variation of the Ge content in the scaffolds strongly determined their mass loss in physiologic conditions. Indeed, the mass loss can be directly assigned to the initial Ge percentage in the nanofibres, that was released during immersion [20]. Hence, the high hydrophilicity and solubility of Ge in aqueous solutions were demonstrated.

Regarding the PAni presence in the nanofibres, a lower remaining mass could be detected as it increased in the composition, especially in the 40/60 PCL/Ge scaffolds for high dissolution time. Although this observation was not critical, it may be hypothesised that the PAni preferably interacted with Ge molecules and highly hydrolysed PCL chains, which were then released during immersion. This observation may suggest that the dispersion of the PAni particles occurs preferably into more hydrophilic domains [96].

Considering the dissolution time, slightly higher mass loss was appreciated for all the compositions as it increased. Therefore, a more pronounced disintegration was perceived for scaffolds prepared after 48 and 72 h of dissolution. This behaviour can be ascribed to the release of low molar mass hydrolytically degraded PCL segments. Finally, the scaffolds electrospun after 96 h were completely disintegrated in all cases during the first 20 days, and mass loss could not be evaluated.

The pH of the degradation media remained between 7 and 7.5 for all the studied compositions after 100 days of immersion, in line with that of the initial PBS solution, adjusted to 7.4. This behaviour corroborated the slow degradation of the PCL molecules in simulated service conditions and highlighted the buffer ability of the PBS for the released acid oligomers from the PCL hydrolysis. Overall, the pH maintenance may suggest that these scaffolds would not cause acute inflammatory reactions due to the possible release of hydrolysed by-products.

The average molar mass in number (M_n) of the PCL fraction was complementarily analysed after 100 days of immersion in simulated physiological conditions. The effect of the dissolution time could only be analysed in the nanofibres obtained after 24, 48, and 72 h of dissolution time. As cited before, those electrospun after 96 h of dissolution could no longer be evaluated. The obtained values of M_n along with the variation in percentage (ΔM_n) are gathered in **Table 4**.

Table 4. Average molar mass in number (M_n) and percentage variation after 100 days in simulated physiological conditions (phosphate-buffered saline (PBS) at 37 ºC).

PCL/Ge	PAni	Dissolution time (h)					
(% wt)	(% wt)	24		48		72	
		M_n (g·mol^{-1})	ΔM_n (%)	M_n (g·mol^{-1})	ΔM_n (%)	M_n (g·mol^{-1})	ΔM_n (%)
60/40	-	16221	-56.87	11121	-49.72	9021	-43.72
	0.50	15498	-53.32	12341	-45.63	8003	-53.58
	1.00	13936	-60.26	13109	-42.12	8493	-49.83
50/50	-	14575	-62.77	8628	-62.26	7080	-56.75
	0.50	13242	-61.81	8953	-56.56	7613	-55.09
	1.00	13728	-63.24	9152	-57.61	7081	-57.37
40/60	-	13352	-64.91	6896	-69.89	6761	-52.35
	0.50	10220	-70.50	7338	-69.74	6041	-57.19
	1.00	11863	-65.76	8874	-60.33	6165	-57.66

The average molar mass in number (M_n) generally decreased from 15000 to 6000 g·mol^{-1}. This molar mass decrease (ΔM_n) of the PCL was found in the range from 70 to 45% due to the hydrolytic chain scission during immersion in simulated physiologic conditions. Although high dispersion was found in the results, it may be intuited a more significant degradation for higher Ge composition and shorter dissolution time. On the one hand, the higher proportion of the hydrolytic media in comparison to the percentage of PCL along with the predominant amorphous structure revealed before for rich-Ge scaffolds may be responsible for this performance. On the other hand, higher degradation could be perceived the lower was the dissolution time before electrospinning. In the less hydrolytically degraded PCL during processing (24 h of dissolution time), the molar mass decrease was more significant (around 10%) than in the nanofibres electrospun after higher dissolution time (72 h) regardless of the composition. The PCL chains with a higher molar mass showed a greater number of ester bonds available for being hydrolysed. According to the exponential decreasing pattern suggested in the previous section, the less degraded segments during processing may have a higher margin for being hydrolytically degraded in simulated physiologic conditions. Overall, even though these small differences were highlighted, such scaffolds with this low molar mass of the PCL fraction would be completely resorbed in a short period (<15 days) during *in vivo* subdermal or heart implantation [13].

3.5. In vitro biocompatibility

The influence of the PCL-to-Ge ratio and, especially the effect of PAni on the biocompatibility of the scaffolds was assessed in the electrospun nanofibres after 24 and 48 h of dissolution time.

3.5.1. Cell proliferation

The biocompatibility of the scaffolds was firstly assessed through *the in vitro MTT cell proliferation assay* by comparing the absorbance at 550 nm after 48 h and 96 h of cell culture [13,97]. The normalised cell proliferation rates (in comparison to the PCL/Ge scaffolds without PAni, electrospun after 24 h) are plotted in **Figure 11** as the ratio of cells measured at 96 h divided by those found after 48 h.

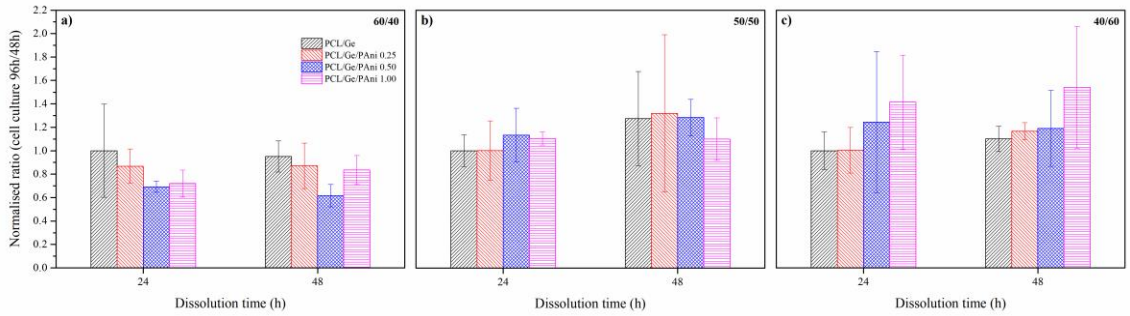

Figure 11. Normalised cell culture ratio for the 60/40, 50/50, and 40/60 PCL/Ge scaffolds as a function of the PAni content and dissolution time. Plots are labelled according to the PCL/Ge composition as a) 60/40; b) 50/50; and c) 40/60.

In terms of PCL-to-Ge ratio, biocompatibility increased for higher Ge percentages, and therefore the 40/60 PCL/Ge composition was the most biocompatible [13]. The presence of gelatin with its more hydrophilic behaviour and structure containing highly biocompatible Arginyl-Glycyl-Aspartic amino acid sequences (RGD), offered biochemical signals for the adhesion, migration, and proliferation of HL-1 Cells, an immortalized line from murine atrial cardiomyocytes [20].

If compared to their respective PCL/Ge composition, the addition of PAni resulted in dissimilar tendencies. Although all the compositions maintained the proliferative properties of the cells, a particular performance was perceived for each PCL/Ge composition. While for the 60/40 scaffolds the PAni slightly decreased the cell proliferation (10-20%), for the 50/50 the effect was unclear (±10%) and for the 40/60 the PAni contributed to the cell spread. For these compositions with a higher Ge percentage, the presence of PAni boosted proliferation. Indeed, the cell culture ratio progressively increased with the addition of PAni, up to 40% for the 1.00 %wt of these conductive microparticles. Previous works have shown the potential of conductive scaffolds to promote cell attachment and proliferation [36,41].

In general, proliferation rates were slightly better for higher dissolution time, particularly for the 40/60 PCL/Ge scaffolds. The generation of carboxyl groups from hydrolysed PCL molecules may have increased hydrophilicity and therefore biocompatibility of the nanofibres. Although the hydrolytic breakage of PCL changed the nanofibre morphology and microstructure and subsequently determined the biodegradation behaviour of the scaffolds, comparable proliferations ratios were found regardless of the dissolution time.

To visually corroborate the cell attachment to the scaffolds, cells were seeded, fixed after 48 and 96 h of culture, and finally stained with DAPI [98]. The obtained images are shown in **Figure 12** as a function of the PCL/Ge composition, PAni content, and dissolution time. Cells could be observed in all the studied scaffolds. In terms of composition, proliferation increased as a function of the Ge content, given its higher biocompatibility. Indeed, whilst in the 60/40 PCL/Ge composition cells could be hardly observed, in the 40/60 nanofibres the cell population increased and occupied more surface of the scaffolds after 96 h of culture. Regarding the dissolution time, similar images were obtained both for scaffolds electrospun after 24 and 48 h. All these results were in line with those previously described for the MTT assay.

The presence of PAni was revealed to have not impaired the cellular growth in any of the compositions. Indeed, it could be intuited that when PAni was incorporated into the scaffolds, grouped cell cores were visible. In particular, this behaviour could be observed for the 50/50 and 40/60 PCL/Ge compositions and the highest PAni content (1.00 %wt). These cellular centres may have grouped in the vicinities of the PAni microparticles, which allowed for stimulation through successful beating propagation.

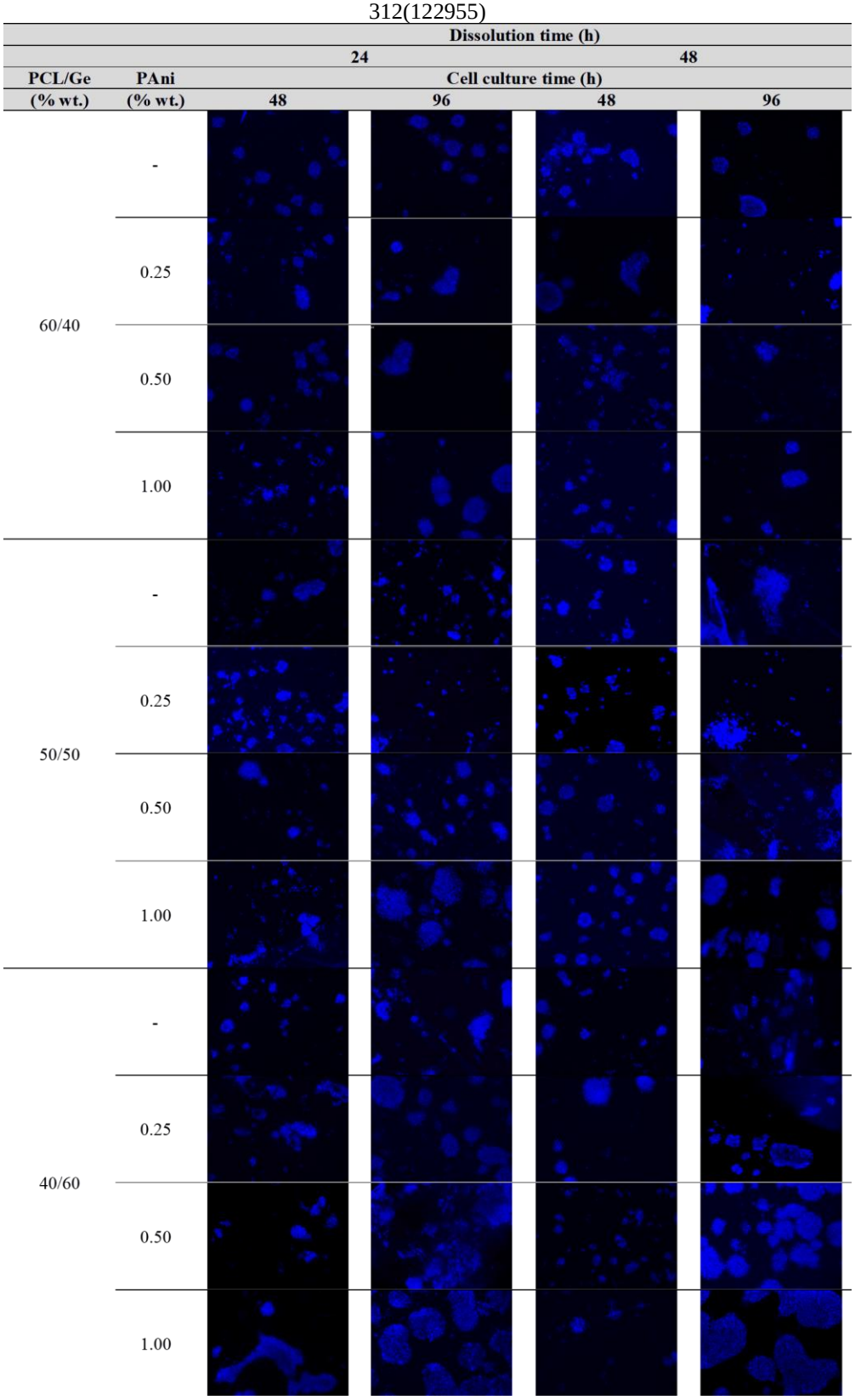

Figure 12. Nuclear staining with DAPI during culture (48 and 96 h) of 40000 cells·cm^{-2} onto the 60/40, 50/50, and 40/60 PCL/Ge scaffolds with different PAni content as a function of the dissolution time.

3.5.2. Cellular cytotoxicity

Several studies remark the necessity of the combination of more than one method for assessing the *in vitro* biocompatibility with specific cell lines and dissimilar applications [99]. Therefore, the lactate dehydrogenase assay (LDH) was complementarily performed to furtherly characterise the effect of the different PCL/Ge composition and PAni content when in contact with the cells. This enzyme is used as a biomarker of cellular cytotoxicity as it is released into the media from damaged cells. The LDH release was measured in the supernatants 48 h after cells platting and the obtained results are plotted in **Figure 13**. Given that cells grew dissimilarly onto the scaffolds, as shown in previous sections by DAPI nuclear staining, the release of LDH was normalised against the total amount of protein.

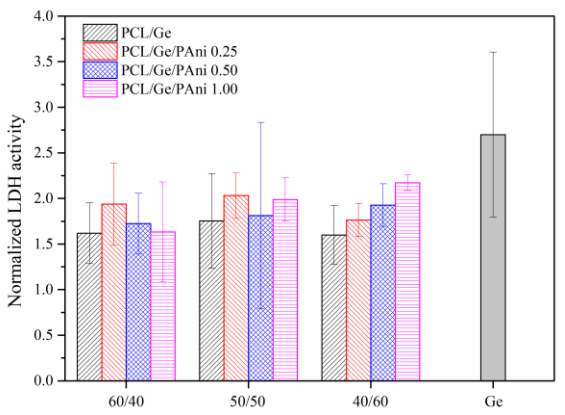

Figure 13. Graphical representation of LDH release assay in HL-1 Cells cultured onto the scaffolds as a function of the PCL/Ge composition and the PAni content. Control cells were seeded in gelatin pre-coated wells. Data were normalised against the total amount of protein.

Non-significant differences in the LDH release were observed regardless of the PCL/Ge composition. Values of protein release in the different scaffolds ranged from 1.60±0.32 to 2.17±0.08, whereas an LDH of 2.70±0.90 was measured in control cells. Although a slightly increasing tendency was found as a function of the PAni content for the LDH measured in the 40/60 scaffolds, it was below that of the control in all cases. Indeed, cells plated onto all the analysed scaffolds released less LDH compared with cells directly platted onto gelatin pre-coated wells. These results are in accordance with previous studies where human umbilical vein endothelial cells were able to grow and proliferate onto PCL/PAni scaffolds without altering the LDH release [100].

3.5.3. Analysis of macrophage M1 and M2 profile

A major hallmark for myocardial infarction is the massive inflammatory cells infiltration into the myocardium layer [101]. Macrophages play a crucial role during disease progression, and macrophages

profiles during cardiac injury determine its satisfactory resolution [36]. It is known that some scaffolds may alter the macrophage polarization so that those which do not alter or promote macrophage polarization through an M2 and reduce the M1 phenotype would be preferred [102].

In this section, the effect of combined PCL, Ge, and PAni on the macrophage profile was ascertained. Therefore, the PCL/Ge/PAni scaffolds with compositions 40/60/1.00, 50/50/1.00, and 60/40/1.00 were cultured and evaluated. In particular, the expression profile of TNFα and CD206 proteins, as expressed by M1 and M2 type macrophages respectively, were analysed through qPCR, and the obtained results are plotted in **Figure 14**.

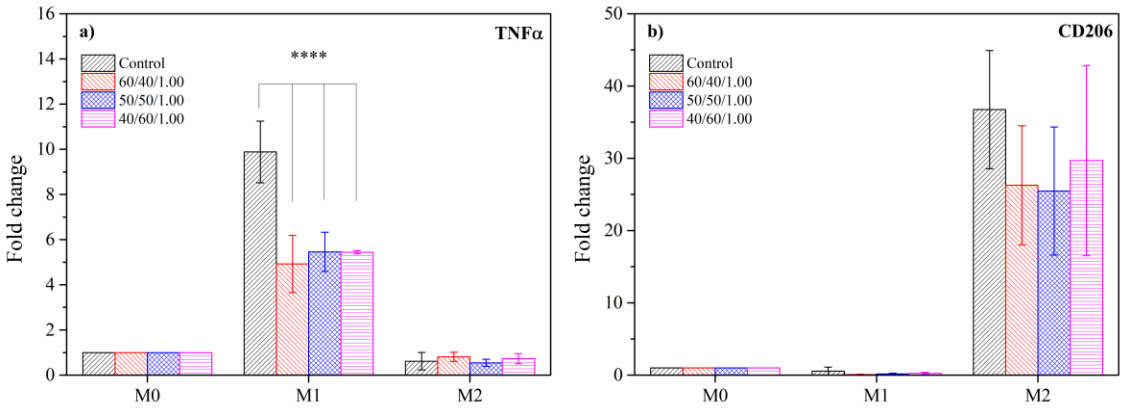

Figure 14. Gene expression associated with a) M1 (TNFα), and b) M2 (CD206) markers. GAPDH was used as a reference gene for normalisation. ****$p < 0.0001$.

In general, results revealed that none of the scaffolds impaired macrophage polarization. On the one hand, significant differences were observed between the control and cells seeded onto the scaffolds when assessing the change in TNFα, which is a specific marker of the M1 profile. Macrophages seeded on scaffolds containing PAni (1.00 %wt) showed less expression of the proinflammatory cytokine TNFα than control cells. Moreover, all the analysed compositions revealed an analogous behaviour, so that the contribution of the different percentages of PCL and Ge was negligible. On the other hand, a similar tendency was observed when assessing CD206, a specific marker of the M2 profile, in which non-relevant differences were observed between cells used as control cells and those seeded onto the scaffolds.

4. Conclusions

Tailored functionalised nanofibrous PCL/Ge/PAni scaffolds were prepared through electrospinning after dissolution into a formic/acetic acid mixture. The relative PCL-to-Ge ratio, the addition of PAni, and the extent of the dissolution time in the hydrolytic acid solvent were considered as key parameters for the design of the nanofibres in terms of morphology, molar mass and crystalline structure. Particularly, the addition of PAni up to 1.00 %wt preserved structural and morphological features and offered a positive functionalisation in terms of controlled increase of electric conductivity.

The *in vitro* evaluation revealed degradation during immersion in physiologic conditions, which could be modulated through the scaffold composition and the dissolution time. Complementary MTT and LDH assays revealed high biocompatibility and non-cytotoxicity. Scaffolds were able to maintain cells in a proliferative state and preserve cardiomyocytes in culture. Moreover, the addition of PAni (1.00 %wt) and the higher presence of Ge enhanced cell proliferation and allowed for the generation of cellular centres, without altering the polarization profile of the macrophage. Considering the benefits of PAni in the increase of conductivity, and the promising signs in terms of biocompatibility, it may be stated that the 40/60/1.00 PCL/Ge/PAni scaffold is the best candidate for the proliferation of HL-1 Cells with potential uses in the cardiac tissue engineering field. Further studies will allow for understanding the role of PAni to modulate the electrophysiological properties of cardiomyocytes.

Acknowledgements

Generalitat Valenciana is thanked for the post-doctoral contracts of O. Gil-Castell (APOSTD/2020/155) and I. Ontoria-Oviedo (CDPT-01/20-A). The ISCIII is acknowledged for the RETICS Program (RD16/0011/0004) as well as for the grant PI19/00245, co-funded by the European Regional Development Fund-ERDF. Dr. M. Orzáez is recognised for kindly providing the THP-1 Cells (Centro de Investigación Príncipe Felipe, Valencia, Spain). Finally, the authors recognise the microscopy and cell cultures core facilities of UPV and IIS La Fe for their grateful collaboration.

Data availability

The raw/processed data required to reproduce these findings cannot be shared at this time as the data also forms part of an ongoing study.

References

[1] S. Stratton, N.B. Shelke, K. Hoshino, S. Rudraiah, S.G. Kumbar, Bioactive polymeric scaffolds for tissue engineering, Bioact. Mater. 1 (2016) 93–108. doi:10.1016/J.BIOACTMAT.2016.11.001.

[2] S. Agarwal, A. Greiner, J.H. Wendorff, Functional materials by electrospinning of polymers, Prog. Polym.

Sci. 38 (2013) 963–991. doi:10.1016/j.progpolymsci.2013.02.001.

[3] Hanumantharao, Rao, Multi-Functional Electrospun Nanofibers from Polymer Blends for Scaffold Tissue Engineering, Fibers. 7 (2019) 66. doi:10.3390/fib7070066.

[4] S. Pisani, R. Dorati, B. Conti, T. Modena, G. Bruni, I. Genta, Design of copolymer PLA-PCL electrospun matrix for biomedical applications, React. Funct. Polym. 124 (2018) 77–89. doi:10.1016/j.reactfunctpolym.2018.01.011.

[5] A. Oner, E. Tufek, I. Yezer, A. Birol, M. Demir, S. Er, D.O. Demirkol, High generation dendrimer decorated poly-Ɛ-caprolactone/polyacrylic acid electrospun nanofibers for the design of a bioelectrochemical sensing surface, React. Funct. Polym. 161 (2021) 104853. doi:10.1016/j.reactfunctpolym.2021.104853.

[6] D. Simões, S.P. Miguel, I.J. Correia, Biofunctionalization of electrospun poly(caprolactone) fibers with Maillard reaction products for wound dressing applications, React. Funct. Polym. 131 (2018) 191–202. doi:10.1016/j.reactfunctpolym.2018.07.021.

[7] K. Ghosal, R. Augustine, A. Zaszczynska, M. Barman, A. Jain, A. Hasan, N. Kalarikkal, P. Sajkiewicz, S. Thomas, Novel drug delivery systems based on triaxial electrospinning based nanofibers, React. Funct. Polym. 163 (2021) 104895. doi:10.1016/j.reactfunctpolym.2021.104895.

[8] X. Li, Z. Chen, H. Zhang, Y. Zhuang, H. Shen, Y. Chen, Y. Zhao, B. Chen, Z. Xiao, J. Dai, Aligned scaffolds with biomolecular gradients for regenerative medicine, Polymers (Basel). 11 (2019). doi:10.3390/polym11020341.

[9] A. Haider, S. Haider, I.-K.K. Kang, A comprehensive review summarizing the effect of electrospinning parameters and potential applications of nanofibers in biomedical and biotechnology, Arab. J. Chem. In press (2015) 1165–1188. doi:10.1016/j.arabjc.2015.11.015.

[10] D.I. Braghirolli, D. Steffens, P. Pranke, Electrospinning for regenerative medicine: a review of the main topics, Drug Discov. Today. 19 (2014) 743–753. doi:10.1016/j.drudis.2014.03.024.

[11] O. Gil-Castell, J.D.J.D. Badia, J. Bou, A. Ribes-Greus, Performance of polyester-based electrospun scaffolds under in vitro hydrolytic conditions: From short-term to long-term applications, Nanomaterials. 9 (2019) 786. doi:10.3390/nano9050786.

[12] O. Gil-Castell, J.D. Badia, E. Strömberg, S. Karlsson, A. Ribes-Greus, Effect of the dissolution time into an acid hydrolytic solvent to tailor electrospun nanofibrous polycaprolactone scaffolds, Eur. Polym. J. 87 (2017) 174–187. doi:10.1016/j.eurpolymj.2016.12.005.

[13] O. Gil-Castell, J.D.D. Badia, I. Ontoria-Oviedo, D. Castellano, P. Sepúlveda, A. Ribes-Greus, Polycaprolactone/gelatin-based scaffolds with tailored performance: in vitro and in vivo validation, Mater. Sci. Eng. C. 107 (2020). doi:10.1016/j.msec.2019.110296.

[14] O. Gil-Castell, J.D.D. Badia, A. Ribes-Greus, Tailored electrospun nanofibrous polycaprolactone/gelatin scaffolds into an acid hydrolytic solvent system, Eur. Polym. J. 101 (2018) 273–281. doi:10.1016/j.eurpolymj.2018.02.030.

[15] M.A. Woodruff, D.W. Hutmacher, The return of a forgotten polymer—Polycaprolactone in the 21st century, Prog. Polym. Sci. 35 (2010) 1217–1256. doi:10.1016/j.progpolymsci.2010.04.002.

[16] A. Cipitria, A. Skelton, T.R. Dargaville, P.D. Dalton, D.W. Hutmacher, Design, fabrication and characterization of PCL electrospun scaffolds—a review, J. Mater. Chem. 93 (2011) 1539–1550. doi:10.1039/c0jm04502k.

[17] X. Wang, H. Zhao, L.S. Turng, Q. Li, Crystalline morphology of electrospun poly(e-caprolactone) (PCL) nanofibers, Ind. Eng. Chem. Res. 52 (2013) 4939–4949. doi:10.1021/ie302185e.

[18] L. Bosworth, P. Clegg, S. Downes, Electrospun nanofibres of polycaprolactone, and their use for tendon regeneration, Int. J. Nano Biomater. 1 (2008) 263. doi:10.1504/IJNBM.2008.016875.

[19] Y. Mao, N. Sanbhal, Y. Li, C. Yu, F. Wang, R. Guidoin, J. Gao, L. Wang, Chitosan functionalised poly(ε-caprolactone) nanofibrous membranes as potential anti-adhesive barrier films, React. Funct. Polym. 143 (2019) 104319. doi:10.1016/j.reactfunctpolym.2019.104319.

[20] Q. Jiang, H. Xu, S. Cai, Y. Yang, Ultrafine fibrous gelatin scaffolds with deep cell infiltration mimicking 3D ECMs for soft tissue repair, J. Mater. Sci. Mater. Med. 25 (2014) 1789–1800. doi:10.1007/s10856-014-5208-2.

[21] R.S. Tığlı, N.M. Kazaroğlu, B. Mavış, M. Gümüşderelioğlu, Cellular Behavior on Epidermal Growth Factor (EGF)-Immobilized PCL/Gelatin Nanofibrous Scaffolds, J. Biomater. Sci. Polym. Ed. 22 (2011) 207–223. doi:10.1163/092050609X12591500475424.

[22] L.H. Chong, M.M. Lim, N. Sultana, Fabrication and Evaluation of Polycaprolactone / Gelatin-Based Electrospun Nanofibers with Antibacterial Properties, J. Nanomater. 2015 (2015) 1–8. doi:10.1155/2015/970542.

[23] H. Duan, B. Feng, X. Guo, J. Wang, L. Zhao, G. Zhou, W. Liu, Y. Cao, W.J. Zhang, Engineering of epidermis skin grafts using electrospun nanofibrous gelatin/polycaprolactone membranes, Int. J. Nanomedicine. 8 (2013) 2077–2084. doi:10.2147/IJN.S42384.

[24] S. Gautam, C.-F. Chou, A.K. Dinda, P.D. Potdar, N.C. Mishra, Surface modification of nanofibrous polycaprolactone/gelatin composite scaffold by collagen type I grafting for skin tissue engineering, Mater. Sci. Eng. C. 34 (2014) 402–409. doi:10.1016/j.msec.2013.09.043.

[25] M.S. Kim, I. Jun, Y.M. Shin, W. Jang, S.I. Kim, H. Shin, The Development of Genipin-Crosslinked Poly(caprolactone) (PCL)/Gelatin Nanofibers for Tissue Engineering Applications, Macromol. Biosci. 10 (2010) 91–100. doi:10.1002/mabi.200900168.

[26] S. Heydarkhan-Hagvall, K. Schenke-Layland, A.P. Dhanasopon, F. Rofail, H. Smith, B.M. Wu, R. Shemin, R.E. Beygui, W.R. MacLellan, Three-dimensional electrospun ECM-based hybrid scaffolds for cardiovascular tissue engineering, Biomaterials. 29 (2008) 2907–2914. doi:10.1016/j.biomaterials.2008.03.034.

[27] S. Pok, J.D. Myers, S. V. Madihally, J.G. Jacot, A multilayered scaffold of a chitosan and gelatin hydrogel supported by a PCL core for cardiac tissue engineering, Acta Biomater. 9 (2013) 5630–5642. doi:10.1016/j.actbio.2012.10.032.

[28] M.A. Alvarez-Perez, V. Guarino, V. Cirillo, L. Ambrosio, Influence of Gelatin Cues in PCL Electrospun Membranes on Nerve Outgrowth, Biomacromolecules. 11 (2010) 2238–2246. doi:10.1021/bm100221h.

[29] D. Gupta, J. Venugopal, M.P. Prabhakaran, V.R.G. Dev, S. Low, A.T. Choon, S. Ramakrishna, Aligned and random nanofibrous substrate for the in vitro culture of Schwann cells for neural tissue engineering, Acta Biomater. 5 (2009) 2560–2569. doi:10.1016/j.actbio.2009.01.039.

[30] I. Rajzer, E. Menaszek, R. Kwiatkowski, J.A. Planell, O. Castano, Electrospun gelatin/poly(ε-caprolactone) fibrous scaffold modified with calcium phosphate for bone tissue engineering, Mater. Sci. Eng. C. 44 (2014) 183–190. doi:10.1016/j.msec.2014.08.017.

[31] M.A. Alvarez Perez, V. Guarino, V. Cirillo, L. Ambrosio, In vitro mineralization and bone osteogenesis in poly(ε-caprolactone)/gelatin nanofibers, J. Biomed. Mater. Res. Part A. 100A (2012) 3008–3019. doi:10.1002/jbm.a.34233.

[32] A.K. Jaiswal, H. Chhabra, V.P. Soni, J.R. Bellare, Enhanced mechanical strength and biocompatibility of electrospun polycaprolactone-gelatin scaffold with surface deposited nano-hydroxyapatite, Mater. Sci. Eng. C. 33 (2013) 2376–2385. doi:10.1016/j.msec.2013.02.003.

[33] R.S. Azarudeen, M.N. Hassan, M.A. Yassin, M. Thirumarimurugan, N. Muthukumarasamy, D. Velauthapillai, K. Mustafa, 3D printable Polycaprolactone-gelatin blends characterized for in vitro osteogenic potency, React. Funct. Polym. 146 (2020) 104445. doi:10.1016/j.reactfunctpolym.2019.104445.

[34] R. Zheng, H. Duan, J. Xue, Y.Y. Liu, B. Feng, S. Zhao, Y. Zhu, Y.Y. Liu, A. He, W. Zhang, W. Liu, Y. Cao, G. Zhou, The influence of Gelatin/PCL ratio and 3-D construct shape of electrospun membranes on cartilage regeneration, Biomaterials. 35 (2014) 152–164. doi:10.1016/j.biomaterials.2013.09.082.

[35] B. Guo, B. Lei, P. Li, P.X. Ma, Functionalized scaffolds to enhance tissue regeneration, Regen. Biomater. 2 (2015) 47–57. doi:10.1093/rb/rbu016.

[36] R. Dong, P.X. Ma, B. Guo, Conductive biomaterials for muscle tissue engineering, Biomaterials. 229 (2020).

doi:10.1016/j.biomaterials.2019.119584.

[37] J.Y. Lee, C.A. Bashur, A.S. Goldstein, C.E. Schmidt, Polypyrrole-coated electrospun PLGA nanofibers for neural tissue applications, Biomaterials. 30 (2009) 4325–4335. doi:10.1016/J.BIOMATERIALS.2009.04.042.

[38] D.D. Ateh, H.A. Navsaria, P. Vadgama, Polypyrrole-based conducting polymers and interactions with biological tissues., J. R. Soc. Interface. 3 (2006) 741–52. doi:10.1098/rsif.2006.0141.

[39] G. Shi, M. Rouabhia, S. Meng, Z. Zhang, Electrical stimulation enhances viability of human cutaneous fibroblasts on conductive biodegradable substrates, J. Biomed. Mater. Res. Part A. 84A (2008) 1026–1037. doi:10.1002/jbm.a.31337.

[40] A.-D. Bendrea, L. Cianga, I. Cianga, Review paper: Progress in the Field of Conducting Polymers for Tissue Engineering Applications, J. Biomater. Appl. 26 (2011) 3–84. doi:10.1177/0885328211402704.

[41] B. Guo, P.X. Ma, Conducting Polymers for Tissue Engineering, Biomacromolecules. 19 (2018) 1764–1782. doi:10.1021/ACS.BIOMAC.8B00276.

[42] B. Zhang, J. He, M. Shi, Y. Liang, B. Guo, Injectable self-healing supramolecular hydrogels with conductivity and photo-thermal antibacterial activity to enhance complete skin regeneration, Chem. Eng. J. 400 (2020) 125994. doi:10.1016/j.cej.2020.125994.

[43] R. Balint, N.J. Cassidy, S.H. Cartmell, Conductive polymers: Towards a smart biomaterial for tissue engineering, Acta Biomater. 10 (2014) 2341–2353. doi:10.1016/J.ACTBIO.2014.02.015.

[44] B. Guo, L. Glavas, A.-C. Albertsson, Biodegradable and electrically conducting polymers for biomedical applications, Prog. Polym. Sci. 38 (2013) 1263–1286. doi:10.1016/j.progpolymsci.2013.06.003.

[45] K.A. Ibrahim, Synthesis and characterization of polyaniline and poly(aniline-co-o-nitroaniline) using vibrational spectroscopy, Arab. J. Chem. 10 (2017) S2668–S2674. doi:10.1016/j.arabjc.2013.10.010.

[46] R. Fryczkowski, T. Kowalczyk, Nanofibres from polyaniline/polyhydroxybutyrate blends, Synth. Met. 159 (2009) 2266–2268. doi:10.1016/j.synthmet.2009.09.008.

[47] J.C.C. Wu, S. Ray, M. Gizdavic-Nikolaidis, B. Uy, S. Swift, J. Jin, R.P. Cooney, Nanostructured bioactive material based on polycaprolactone and polyaniline fiber-scaffolds, Synth. Met. 198 (2014) 41–50. doi:10.1016/j.synthmet.2014.09.017.

[48] M. Khalid, A.M.B. Honorato, H. Varela, Polyaniline: Synthesis Methods, Doping and Conduction Mechanism, Polyaniline - From Synth. to Pract. Appl. (2018) 1–17. doi:http://dx.doi.org/10.5772/intechopen.79089.

[49] R. Ravichandran, S. Sundarrajan, J.R. Venugopal, S. Mukherjee, S. Ramakrishna, Applications of conducting polymers and their issues in biomedical engineering, J. R. Soc. Interface. 7 (2010) S559–S579. doi:10.1098/rsif.2010.0120.focus.

[50] P. Zarrintaj, I. Rezaeian, B. Bakhshandeh, B. Heshmatian, M.R. Ganjali, Bio - Conductive Scaffold Based on Agarose - Polyaniline for Tissue Engineering, J. Ski. Stem Cell. In Press (2017) 4–7. doi:10.5812/jssc.67394.

[51] G. Boara, M. Sparpaglione, Synthesis of polyanilines with high electrical conductivity, Synth. Met. 72 (1995) 135–140. doi:10.1016/0379-6779(94)02337-X.

[52] M. Li, Y. Guo, Y. Wei, A.G. MacDiarmid, P.I. Lelkes, Electrospinning polyaniline-contained gelatin nanofibers for tissue engineering applications, Biomaterials. 27 (2006) 2705–2715. doi:10.1016/J.BIOMATERIALS.2005.11.037.

[53] T.H. Qazi, R. Rai, A.R. Boccaccini, Tissue engineering of electrically responsive tissues using polyaniline based polymers: A review, Biomaterials. 35 (2014) 9068–9086. doi:10.1016/J.BIOMATERIALS.2014.07.020.

[54] J. Chen, M. Yu, B. Guo, P.X. Ma, Z. Yin, Conductive nanofibrous composite scaffolds based on in-situ formed polyaniline nanoparticle and polylactide for bone regeneration, J. Colloid Interface Sci. 514 (2018) 517–527. doi:10.1016/j.jcis.2017.12.062.

[55] J.E. Mark, ed., Properties of Polymers Handbook, Second Edi, Springer, New York, 2007.

[56] J.L. Lauritzen, J.D. Hoffman, Theory of polymer crystals with folded chains in dilute solution, J. Res. Natl. Bur. Stand. 64A (1960) 73.

[57] J.D. Hoffman, J.I. Lauritzen, Crystallization of Bulk Polymers With Chain Folding : Theory of Growth of Lamellar Spherulites, J. Res. Natl. Bur. Stand. - A. Phys. Chem. 65 (1961) 1961. doi:10.6028/jres.065A.035.

[58] J.D. Hoffman, G.T. Davis, J.I. Lauritzen, Crystalline and noncrystalline solids, New York, 1976. doi:10.1007/978-1-4684-2664-9.

[59] O. Gil-Castell, J.D. Badia, R. Teruel-Juanes, I. Rodriguez, F. Meseguer, A. Ribes-Greus, Novel silicon microparticles to improve sunlight stability of raw polypropylene, Eur. Polym. J. 70 (2015) 247–261. doi:10.1016/j.eurpolymj.2015.06.031.

[60] Y. Suzuki, H. Duran, W. Akram, M. Steinhart, G. Floudas, H.-J. Butt, Multiple nucleation events and local dynamics of poly(ε-caprolactone) (PCL) confined to nanoporous alumina, Soft Matter. 9 (2013) 9189. doi:10.1039/c3sm50907a.

[61] ISO, ISO10993-13 Biological evaluation of medical devices - Part 13: Identification and quantification of degradation products from polymeric medical devices, 2010.

[62] O. Gil-Castell, J.D. Badia, I. Ontoria-Oviedo, D. Castellano, B. Marco, A. Rabal, J.J. Bou, A. Serra, L. Monreal, M. Blanes, P. Sepúlveda, A. Ribes-Greus, In vitro validation of biomedical polyester-based scaffolds: Poly(lactide-co-glycolide) as model-case, Polym. Test. 66 (2018) 256–267. doi:10.1016/j.polymertesting.2018.01.027.

[63] P.L. Graney, S. Ben-Shaul, S. Landau, A. Bajpai, B. Singh, J. Eager, A. Cohen, S. Levenberg, K.L. Spiller, Macrophages of diverse phenotypes drive vascularization of engineered tissues, Sci. Adv. 6 (2020) eaay6391. doi:10.1126/sciadv.aay6391.

[64] K.M. Zurick, M. Bernards, Recent biomedical advances with polyampholyte polymers, J. Appl. Polym. Sci. 131 (2014) n/a-n/a. doi:10.1002/app.40069.

[65] S. Gautam, A.K. Dinda, N.C. Mishra, Fabrication and characterization of PCL/gelatin composite nanofibrous scaffold for tissue engineering applications by electrospinning method, Mater. Sci. Eng. C. 33 (2013) 1228–1235. doi:10.1016/j.msec.2012.12.015.

[66] N.S. Binulal, A. Natarajan, D. Menon, V.K. Bhaskaran, U. Mony, S. V. Nair, PCL-gelatin composite nanofibers electrospun using diluted acetic acid-ethyl acetate solvent system for stem cell-based bone tissue engineering, J. Biomater. Sci. Polym. Ed. 25 (2014) 325–340. doi:10.1080/09205063.2013.859872.

[67] A. Bahadur, A. Saeed, S. Iqbal, M. Shoaib, M.S. ur Rahman, M.I. Bashir, M. Asghar, M.A. Ali, T. Mahmood, Biocompatible waterborne polyurethane-urea elastomer as intelligent anticancer drug release matrix: A sustained drug release study, React. Funct. Polym. 119 (2017) 57–63. doi:10.1016/J.REACTFUNCTPOLYM.2017.08.001.

[68] A. Bahadur, M. Shoaib, S. Iqbal, A. Saeed, M.S. ur Rahman, P.A. Channar, Regulating the anticancer drug release rate by controlling the composition of waterborne polyurethane, React. Funct. Polym. 131 (2018) 134–141. doi:10.1016/J.REACTFUNCTPOLYM.2018.07.014.

[69] A. Bahadur, A. Saeed, M. Shoaib, S. Iqbal, S. Anwer, Modulating the burst drug release effect of waterborne polyurethane matrix by modifying with polymethylmethacrylate, J. Appl. Polym. Sci. 136 (2019) 47253. doi:10.1002/APP.47253.

[70] J. Yong-Chao, J. Lin, H. An, W. Xiao-Feng, L. Qian, T. Lih-Sheng, Electrospun polycaprolactone/gelatin composites with enhanced cell–matrix interactions as blood vessel endothelial layer scaffolds, Mater. Sci. Eng. C. 71 (2017) 901–908. doi:10.1016/J.MSEC.2016.10.083.

[71] S. Krimm, J. Bandekar, Vibrational spectroscopy and conformation of peptides, polypeptides, and proteins., Adv. Protein Chem. 38 (1986) 181–364. http://www.ncbi.nlm.nih.gov/pubmed/3541539 (accessed April 28, 2018).

[72] M. Shaban, M. Rabia, A.M.A. El-Sayed, A. Ahmed, S. Sayed, Photocatalytic properties of PbS/graphene oxide/polyaniline electrode for hydrogen generation, Sci. Rep. 7 (2017) 14100. doi:10.1038/s41598-017-14582-8.

[73] D. Kolbuk, P. Sajkiewicz, P. Denis, E. Choinska, Investigations of polycaprolactone/gelatin blends in terms of their miscibility, Bull. Polish Acad. Sci. Tech. Sci. 61 (2013) 629–632. doi:10.2478/bpasts-2013-0066.

[74] S. Gautam, C.C. Amit, K. Dinda, Fabrication and characterization of PCL / gelatin / chitosan ternary nanofibrous composite scaffold for tissue engineering applications, J. Mater. Sci. 49 (2014) 1076–1089. doi:10.1007/s10853-013-7785-8.

[75] S.Amadori, P. Torricelli, K. Rubini, M. Fini, S. Panzavolta, A. Bigi, S. Amadori, P. Torricelli, K. Rubini, M. Fini, S. Panzavolta, A. Bigi, Effect of sterilization and crosslinking on gelatin films, J. Mater. Sci. Mater. Med. 26 (2015) 1–9. doi:10.1007/s10856-015-5396-4.

[76] R. Ansari, M.B. Keivani, Polyaniline Conducting Electroactive Polymers: Thermal and Environmental Stability Studies, 2006. http://www.e-journals.net (accessed March 25, 2020).

[77] N. Chandrakanthi, M.A. Careem, Thermal stability of polyaniline, 2000.

[78] L.A. Smith, P.X. Ma, Nano-fibrous scaffolds for tissue engineering, Colloids Surfaces B Biointerfaces. 39 (2004) 125–131. doi:10.1016/j.colsurfb.2003.12.004.

[79] L. Ghasemi-Mobarakeh, M.P. Prabhakaran, M. Morshed, M.-H. Nasr-Esfahani, S. Ramakrishna, Electrospun poly(ε-caprolactone)/gelatin nanofibrous scaffolds for nerve tissue engineering, Biomaterials. 29 (2008) 4532–4539. doi:10.1016/j.biomaterials.2008.08.007.

[80] K. Ren, Y. Wang, T. Sun, W. Yue, H. Zhang, Electrospun PCL/gelatin composite nanofiber structures for effective guided bone regeneration membranes, Mater. Sci. Eng. C. 78 (2017) 324–332. doi:10.1016/J.MSEC.2017.04.084.

[81] D. Kołbuk, P. Sajkiewicz, K. Maniura-Weber, G. Fortunato, Structure and morphology of electrospun polycaprolactone/gelatine nanofibres, in: Eur. Polym. J., Pergamon, 2013: pp. 2052–2061. doi:10.1016/j.eurpolymj.2013.04.036.

[82] D.G. Yu, Y. Xu, Z. Li, L.P. Du, B.G. Zhao, X. Wang, Coaxial electrospinning with mixed solvents: From flat to round eudragit l100 nanofibers for better colon-targeted sustained drug release profiles, J. Nanomater. 2014 (2014). doi:10.1155/2014/967295.

[83] B. Feng, H. Tu, H. Yuan, H. Peng, Y. Zhang, Acetic-acid-mediated miscibility toward electrospinning homogeneous composite nanofibers of GT/PCL, Biomacromolecules. 13 (2012) 3917–3925. doi:10.1021/bm3009389.

[84] J.L. Gornall, E.M. Terentjev, Helix-coil transition of gelatin: Helical morphology and stability, Soft Matter. 4 (2008) 544–549. doi:10.1039/b713075a.

[85] V. Guarino, V. Cirillo, P. Taddei, M.A. Alvarez-Perez, L. Ambrosio, Tuning size scale and crystallinity of PCL electrospun fibres via solvent permittivity to address hMSC response, Macromol. Biosci. 11 (2011) 1694–1705. doi:10.1002/mabi.201100204.

[86] N. Lavielle, A.M. Popa, M. De Geus, A. Hébraud, G. Schlatter, L. Thöny-Meyer, R.M. Rossi, Controlled formation of poly(ε-caprolactone) ultrathin electrospun nanofibers in a hydrolytic degradation-assisted process, Eur. Polym. J. 49 (2013) 1331–1336. doi:10.1016/j.eurpolymj.2013.02.038.

[87] H. Fong, I. Chun, D.H. Reneker, Beaded nanofibers formed during electrospinning, in: Polymer (Guildf)., 1999: pp. 4585–4592. doi:10.1016/S0032-3861(99)00068-3.

[88] D.R. Chen, J.Z. Bei, S.G. Wang, Polycaprolactone microparticles and their biodegradation, Polym. Degrad. Stab. 67 (2000) 455–459. doi:10.1016/S0141-3910(99)00145-7.

[89] F. Khan, M. Tanaka, S.R. Ahmad, Fabrication of polymeric biomaterials: a strategy for tissue engineering and medical devices, J. Mater. Chem. B. 3 (2015) 8224–8249. doi:10.1039/C5TB01370D.

[90] O. Gil-Castell, J.D. Badia, T. Kittikorn, E. Strömberg, M. Ek, S. Karlsson, A. Ribes-Greus, E. Strömberg, M. Ek, S. Karlsson, A. Ribes-Greus, Impact of hydrothermal ageing on the thermal stability, morphology and viscoelastic performance of PLA/sisal biocomposites, Polym. Degrad. Stab. 132 (2016) 87–96. doi:10.1016/j.polymdegradstab.2016.03.038.

[91] O. Gil-Castell, J.D. Badia, T. Kittikorn, E. Strömberg, A. Martínez-Felipe, M. Ek, S. Karlsson, A. Ribes-

Greus, Hydrothermal ageing of polylactide/sisal biocomposites. Studies of water absorption behaviour and Physico-Chemical performance, Polym. Degrad. Stab. 108 (2014) 212–222. doi:10.1016/j.polymdegradstab.2014.06.010.

[92] L. Van der Schueren, B. De Schoenmaker, Ö.I. Kalaoglu, K. De Clerck, An alternative solvent system for the steady state electrospinning of polycaprolactone, Eur. Polym. J. 47 (2011) 1256–1263. doi:10.1016/j.eurpolymj.2011.02.025.

[93] G.L. Siparsky, K.J. Voorhees, F. Miao, Hydrolysis of polylactic acid (PLA) and polycaprolactone (PCL) in aqueous acetonitrile solutions: Autocatalysis, J. Environ. Polym. Degrad. 6 (1998) 31–41. doi:10.1023/A:1022826528673.

[94] C.S. Ki, D.H. Baek, K.D. Gang, K.H. Lee, I.C. Um, Y.H. Park, Characterization of gelatin nanofiber prepared from gelatin-formic acid solution, Polymer (Guildf). 46 (2005) 5094–5102. doi:10.1016/j.polymer.2005.04.040.

[95] J.D. Badia, O. Gil-Castell, A. Ribes-Greus, Long-term properties and end-of-life of polymers from renewable resources, Polym. Degrad. Stab. 137 (2017) 35–57. doi:10.1016/j.polymdegradstab.2017.01.002.

[96] D.S. Dhawale, R.R. Salunkhe, V.S. Jamadade, D.P. Dubal, S.M. Pawar, C.D. Lokhande, Hydrophilic polyaniline nanofibrous architecture using electrosynthesis method for supercapacitor application, Curr. Appl. Phys. 10 (2010) 904–909. doi:10.1016/j.cap.2009.10.020.

[97] G. Mosayebi, M. Ejtehadifar, A. Ganji, Evaluating the Proliferation of Human Peripheral Blood Mononuclear Cells Using MTT Assay Nanobody and aptamer as targeting moiety against bacterial toxins: therapeutic and diagnostic applications View project, (2017). doi:10.15171/ijbsm.2017.06.

[98] S. Das, R.S. Jacob, K. Patel, N. Singh, S.K. Maji, Amyloid Fibrils: Versatile Biomaterials for Cell Adhesion and Tissue Engineering Applications, Biomacromolecules. 19 (2018) 1826–1839. doi:10.1021/acs.biomac.8b00279.

[99] G. Fotakis, J.A. Timbrell, In vitro cytotoxicity assays: Comparison of LDH, neutral red, MTT and protein assay in hepatoma cell lines following exposure to cadmium chloride, Toxicol. Lett. 160 (2006) 171–177. doi:10.1016/j.toxlet.2005.07.001.

[100] Y. Li, X. Li, R. Zhao, C.C. Wang, F. Qiu, B. Sun, H. Ji, J. Qiu, C.C. Wang, Enhanced adhesion and proliferation of human umbilical vein endothelial cells on conductive PANI-PCL fiber scaffold by electrical stimulation, Mater. Sci. Eng. C. 72 (2017) 106–112. doi:10.1016/j.msec.2016.11.052.

[101] D.O. Freytes, L. Santambrogio, G. Vunjak-Novakovic, Optimizing Dynamic Interactions between a Cardiac Patch and Inflammatory Host Cells, Cells Tissues Organs. 195 (2012) 171–182. doi:10.1159/000331392.

[102] D. Castellano, M. Blanes, B. Marco, I. Cerrada, A. Ruiz-Saurí, B. Pelacho, M. Araña, J.A. Montero, V. Cambra, F. Prosper, P. Sepúlveda, A Comparison of Electrospun Polymers Reveals Poly(3-Hydroxybutyrate) Fiber as a Superior Scaffold for Cardiac Repair, Stem Cells Dev. 23 (2014) 1479–1490. doi:10.1089/scd.2013.0578.

ANNEX – OPEN ACCESS POLICIES